LIGHT-ASSISTED DRYING (LAD) FOR THE STABILIZATION OF PROTEINS IN
AMORPHOUS TREHALOSE

by

Madison Ann Young

A dissertation submitted to the faculty of
The University of North Carolina at Charlotte
in partial fulfillment of the requirements
for the degree of Doctorate of Philosophy in
Optical Science and Engineering

Charlotte

2018

Approved by:

_____
Dr. Susan Trammell

_____
Dr. Gloria Elliott

_____
Dr. Nathaniel Fried

_____
Dr. Glenn Boreman

_____
Dr. Charles Lee

ABSTRACT

MADISON ANN YOUNG. Light-assisted drying (LAD) for the stabilization of proteins in amorphous trehalose. (Under the direction of DR. SUSAN R. TRAMMELL)

We have developed a new processing method, light-assisted drying (LAD), to create an amorphous trehalose matrix for the stabilization and storage of proteins. A challenge in the development of protein-based assays and therapeutics is preserving the structure of the protein during production and storage. Freeze-drying or freezing are currently the standard for the preservation of proteins, but these methods are expensive and can be challenging in some environments due to a lack of available infrastructure. LAD offers a relatively inexpensive method for drying samples. LAD immobilizes proteins in an anhydrous, amorphous solid that could potentially be stored at supra zero temperatures making this process attractive for use in low resource settings. Proteins suspended in a trehalose solution are dehydrated using near-infrared laser light. The laser radiation accelerates drying and as water is removed the trehalose forms a protective matrix.

Initially we investigated the effect of laser wavelength, processing power, and sample substrate to determine the optimal LAD parameters for fast processing times and low end moisture contents (EMC). We compared the effect of changing processing wavelength, power and resulting sample temperature, and substrate material on the EMC for two near-infrared (NIR) laser sources (1064 nm and 1850 nm). The 1850 nm laser resulted in the lowest EMC (0.03 ± 0.01 gH2O/gDryWeight) after 20 minutes of processing on borosilicate glass microfiber paper. This suggests a storage temperature of 68.3°C.

In the second study, LAD samples were optically characterized with polarized light imaging (PLI), scanning white light interferometry (SWLI), and Raman spectroscopy. PLI was used to look at crystallization kinetics of samples and determine optimal storage relative humidity (RH). PLI showed a 62.5% probability of minor crystallization during LAD processing and negligible crystallization during 14.3±0.5% RH storage. Scanning white light interferometry (SWLI) was used to measure sample thickness. SWLI measured an average maximum sample thickness of 90.81 ±6.53 μm. Raman spectroscopy was used to investigate trehalose distribution across LAD processed samples. No change in Raman spectra indicated that trehalose was present across samples in an amorphous form.

The final study investigated the effect of varying protein concentration and protein size on EMC. Protein concentration and size (as defined by hydrodynamic radius) had no effect on the EMC reached by LAD for the same processing parameters. We also tested the functionality of a model protein, lysozyme after LAD processing with the 1064 nm laser at ~42°C compared to air drying, samples incubated at a temperature comparable to LAD, a control solution kept at 8°C and ambient temperature, and crystallized samples. Both the LAD – 1064 nm samples and various control and damaged samples did not experience any decrease in functionality. This implies that LAD has no unique negative effect on protein function. The LAD – 1850 nm study was performed above lysozymes melt temperature (~80°C). A sample was processed with LAD and also incubated in a water bath at a comparable temperature. The LAD processed sample showed negligible denaturation compared to the incubated sample which experienced partial denaturation.

Overall, we found that LAD produced uniform samples with repeatable EMC that could enable storage of samples at supra zero temperatures without loss of protein functionality. LAD shows potential for use in applications that require the stabilization of proteins. These applications include protein based diagnostics such as micro arrays and rapid detection test strips. Proteins immobilized on these devices could be stored at ambient temperatures. LAD could also be used to stabilize protein therapeutics at ambient temperatures.

DEDICATION

To mom and dad, thank you for pushing me to dream big and never letting me give up, your support and love have made this possible. You are my inspiration every day. And to Pencie, my best friend and little sister, you have always been my rock (pun intended). And finally to Mr. Pickles, I realize you can't read this because you're a dog, but thank you for being my buddy and loving me even though I've been too busy to take you to the dog park.

ACKNOWLEDGMENTS

First and foremost I want to thank my advisor Dr. Susan Trammell. Her knowledge and guidance are the foundation of my research. She has been my mentor since my undergraduate education and was the driving force behind my decision to pursue my doctorate. I am very grateful to have had such a wonderful advisor who made this, sometimes frustrating, endeavor worthwhile and enjoyable.

Second, I would like to thank Dr. Gloria Elliott, Dr. Nathaniel Fried, Dr. Yasin Raja, and Dr. Charles Lee for serving on my dissertation committee. Their expertise have played a critical role in developing my project. Special thanks to Dr. Elliott and Dr. Fried for letting me use equipment and lab space that was integral to my work.

I would also like to thank my fellow lab mates over the past years: Dr. Jason Case for showing me the ropes in my early lab days and Dr. Joseph Peller for making me laugh endlessly in lab. Also, thank you to Andrew Antczak and Amanda Wawak for their assistance in data collection and analysis.

In addition, I would like to thank my high school physics teacher, Lauren Brown, whose passion for science and patience with my struggles in physics put me on this path.

Finally, thank you to all of my family and friends for their support and encouragement.

TABLE OF CONTENTS

LIST OF TABLES

LIST OF FIGURES

LIST OF ABBREVIATIONS

CCD	charge coupled detector
CW	continuous wave
DS	drying solution
EMC	end moisture content
FWHM	full width at half maximum
LAD	light-assisted drying
NIR	near-infrared
PBS	phosphate buffered saline
PLI	polarized light imaging
RH	relative humidity
SA	standard activity
SWLI	scanning white light interferometry

CHAPTER 1: INTRODUCTION

1.1   Motivation

The objective of this project is to develop a processing method to enable long term stabilization of proteins in amorphous trehalose for dry-state storage at supra zero temperatures. The use of proteins in therapeutics and diagnostics has increased dramatically since the introduction of the first recombinant protein therapeutic — human insulin — more than 30 years ago.[1] Since then, advances in the biotechnology field have led to rapid growth in the discovery of protein-based targets.[2] Protein based therapeutics have been developed to treat diseases ranging from arthritis and psoriasis to cancer.[3] Innovation in protein based diagnostic formats, such as lab on chip micro arrays, have been used in autoimmune profiling and cancer research.[4] A challenge in the development of protein-based diagnostics and drugs is maintaining the protein in the folded state during processing and storage.[5–7] The three-dimensional structure of the protein is often responsible for its functional activity.[8–10] Light-assisted drying (LAD) has the potential to provide a processing and storage method for protein-based drugs and diagnostics by forming an amorphous material around the proteins that will maintain their structural conformation, while increasing shelf life by decreasing bioactivity.

Current methods of protein preservation for short term storage are refrigeration or freezing temperatures in solution sometimes with a stabilizing agent (see Table 1).

Table 1: Comparison of different storage techniques and general temperature shelf life guidelines.[11,12]

Storage Technique and Temperature	In Solution (4°C)	Rapid Freezing with Stabilizer (0°C)	In Solution with Stabilizer (-20°C)	Deep Freeze with Stabilizer (-80°C)	Freeze Drying (≤ 4°C)
General Shelf-life	<1 Month	1 Month	<1 Year	Years	Years

Freeze drying, or lyophilization, is the gold standard for long term protein preservation. Samples are pretreated with a lyoprotectant to reduce ice formation and the solution is slow cooled to -50 to -80°C. The sample then undergoes primary drying to facilitate sublimation of ice followed by secondary drying to remove unfrozen water molecules. Not all proteins are stable during freeze drying and those that are still need to be kept at refrigerated or freezing temperatures. It is a complex, time consuming (> 12 hrs), and high cost process.[13] Other groups have investigated methods for the stabilization of these proteins using ionic liquids.[14–16] However, protein stability depends on the type of ionic liquid used.[17] Recently Elliott et al. have had success with microwave-assisted drying of small volume biologics.[18]

We are developing a drying method that utilizes a glass-forming, sugar-based protectant to create a vitrified matrix suitable for storage at elevated temperatures. Near-infrared (NIR) (1-2 µm) wavelength light is used to control the drying rate and thermal history of the samples during processing. The overall goal of this project is to create a processing technique that could be used to preserve proteins in therapeutics and diagnostics at ambient temperatures.

1.2   Amorphous Solids & Anhydrous Preservation

Anhydrous, dry-state, preservation is the process of removing water from solutions that contain glass-forming protectants, such as disaccharide trehalose. As water is removed from the bulk sample, the remaining sugars and salts become concentrated and as long as they do not crystallize, the viscosity increases with progressive water loss until a glassy (amorphous) state is achieved. This process comes from a form of cryptobiosis found to occur in nature called anhydrobiosis, which is the preservation of certain organisms in situations of extreme desiccation, such as tardigrades or baker's yeast (see Figure 1).
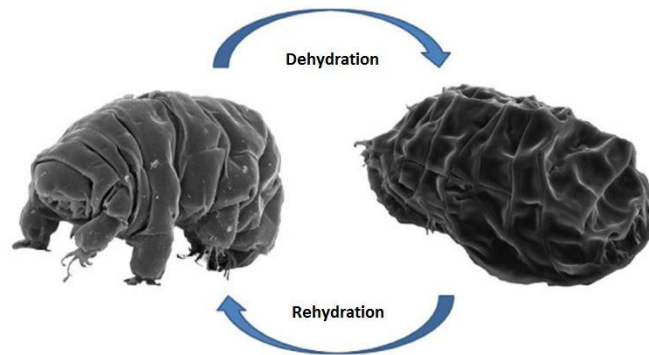
Figure 1: Figure of anhydrobiotic organism, tardigrade.[19]

When these organisms experience desiccation they have been found to produce a sugar called trehalose. It is thought that this sugar stabilizes the organism by forming an amorphous solid, or glass, to protect the organelles. This process is referred to as vitrification.[20]

Recent research has demonstrated that anhydrous, or dry state, preservation in a trehalose amorphous solid matrix may be an alternative to freeze drying for the preservation of biological samples.[21] For example, Crowe et al. have done work based on the idea of anhydrous preservation and have reported successful freeze-drying with trehalose loaded mammalian cells with a 90% survivability.[22] An amorphous solid is a non-crystalline solid such as a glass, plastic or gel. Atoms in a crystalline solid exhibit a property called long-range order; atomic positions repeat in space in a regular lattice. In an amorphous solid, the atoms and molecules are not organized in a lattice pattern (there is no long-range order).[23] An amorphous solid restricts molecular motion to a small volume over a finite time period, which can prevent the degradation of biologics, such as proteins, embedded in the matrix. The regular lattice of a crystalline solid can damage some types of embedded biologics, limiting the usefulness of these solids as preservation matrices.

The main mechanisms for forming an amorphous material are direct solid conversion of the crystal to a glass or transformation of a solution to glass.[24] Our focus is on the transition from liquid to glass. Glass formation requires bypassing crystallization as the solid forms, usually through rapid cooling. Nearly all materials can, if cooled rapidly, form an amorphous solid, but the definition of "rapidly" varies widely among materials. The key to the formation of an amorphous solid is to cool the sample quickly enough to form a glass, instead of slowly to form a crystal. An alternative to rapid cooling is to form the amorphous solid by removing water quickly from a solution to form an amorphous solid preservation matrix. As water is removed from the sample, the remaining sugars and salts become concentrated, and, as long as the solutes do not

crystallize, the viscosity increases with progressive water loss until an amorphous solid is achieved. Disaccharide trehalose can form a low mobility glass (amorphous solid) at room temperature and can also act as a bioprotectant, making trehalose an attractive option as a preservation matrix for embedded biologics.[25] Trehalose is thought to protect biologics during dehydration by compensating for the loss of hydrogen bonding with water on the surface of folded proteins without changing their conformation.[26]

Because a substantial reduction of molecular mobility is necessary to ensure an extended shelf life, samples need to be stored below the glass transition temperature, T_g, of the trehalose matrix to prevent degradation.[27] Below T_g the trehalose maintains its amorphous state. The Gordon-Taylor equation can be used to predict the glass transition temperature (T_g) of trehalose-water mixtures.[28]

$$T_g = \frac{x_1 T_{g,1} + k_{GT}(1 - x_1)T_{g,2}}{x_1 + k_{GT}(1 - x_1)} \quad \text{[Equation 1]}$$

The glass transition temperatures of pure trehalose and pure water are given by $T_{g,1}$ and $T_{g,2}$ respectively, x_1 is the weight fraction of trehalose, and k is an empirically determined fitting parameter. The glass transition temperature for an amorphous trehalose solid formed by dehydration depends on the amount of water remaining in the sample after processing (see Figure 2).
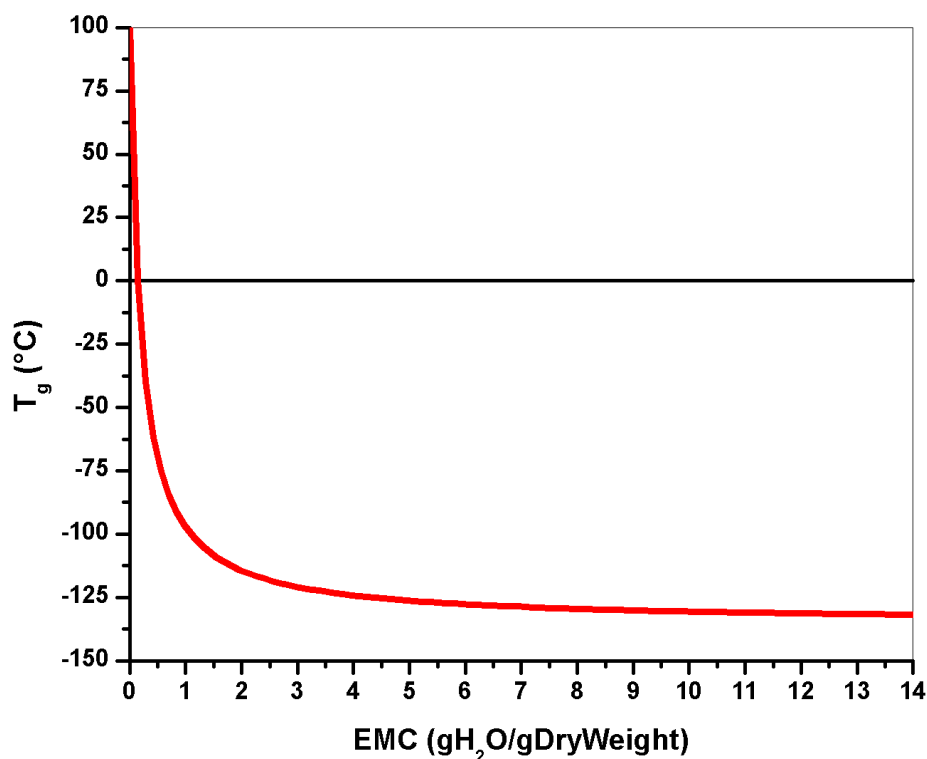
Figure 2: Glass transition curve for a binary mixture of trehalose and water, adapted from the Gordon-Taylor equation for binary solutions of polymers.[29]

The more water that remains in the sample, the lower the glass transition temperature. Lower moisture contents are necessary for storage at higher temperatures. Achieving these low end moisture contents, while maintaining protein functionality, is the key to success for anhydrous preservation methods.

1.3   Light-Assisted Drying (LAD)

We have developed a new processing technique for creating amorphous trehalose solids for the stabilization of proteins in the dry state that uses illumination with near-infrared light to assist in the dehydration of the sample. Laser radiation is routinely used

in a variety of therapeutic procedures in medicine ranging from cataract surgery to tattoo removal.[30],[31] Lasers are the light sources of choice for these procedures as they are monochromatic and collimated, thus can deliver precise amounts of energy to a target. Most therapeutic laser procedures in medicine are based on the idea of selective photothermolysis, which is the precise targeting of chromophores (e.g. water, melanin, hemoglobin and even tattoo ink) in tissue using a specific wavelength of light with the intention of selective absorption of light into a target tissue without absorption in surrounding tissue.[32] The energy directed into the target area produces sufficient heat to damage the target while allowing the surrounding area to remain relatively untouched. For example, blood absorbs light strongly at 530 nm, while absorption due to water (the dominant component of soft tissue) is significantly lower at these wavelengths.[33] Laser treatments of cutaneous hyper vascular malformations such as port-wine stain birthmarks and facial veins exploit the selective absorption of blood. A pulsed laser with wavelength near the 530 nm blood absorption peak heats and coagulates blood vessels, while leaving surrounding water-rich tissue undamaged.[34],[35] We are implementing the principle of selective absorption for dehydration of samples in preparation for anhydrous storage.

Static air-drying of sugar solutions is dominated by evaporative cooling which causes the drying rate to slow substantially. This allows for crystallization of the sugars. We are selectively heating the water in samples of 40µl droplets to overcome cooling due to evaporation and speed dehydration of the samples. NIR light can efficiently transfer energy to water, meaning that when a water-trehalose mixture is illuminated with these wavelengths of light, the sample will absorb energy and heat. Light traveling through a medium can either be scattered or absorbed. In the near-IR spectrum, light absorption is

the dominant effect and the optical penetration depth, δ_P, of the light into a sample can be determined using the absorption coefficient, μ_a. Optical penetration depth is the depth at which light intensity decreases to 1/e of the initial intensity and, when $\mu a \gg \mu_s$, is given by

$$\delta_p \approx \frac{1}{\mu_a} \qquad \text{[Equation 2]}$$

Figure 3 shows the optical penetration depth in water as a function of wavelength.
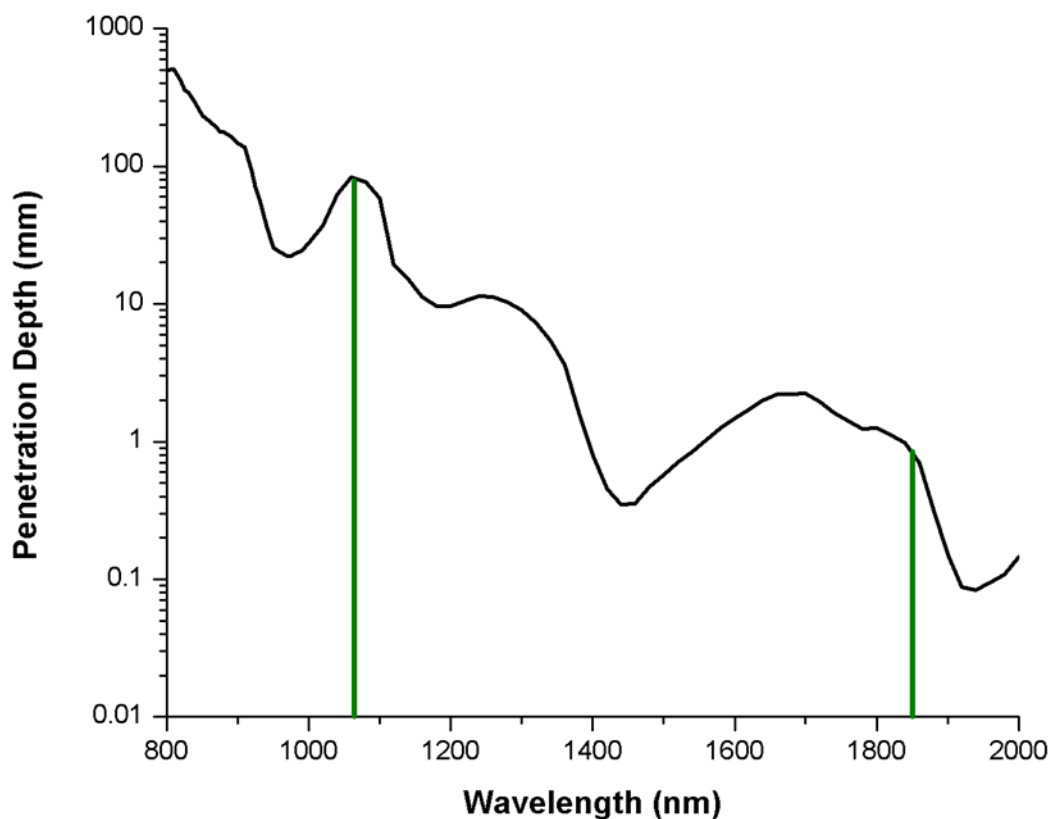
Figure 3: Optical penetration depth in water as a function of wavelength. Both LAD wavelengths are denoted in green.[36]

We have chosen to use laser sources at 1064 nm and 1850 nm wavelengths to heat water to enhance evaporation. The maximum sample thickness used in this study was approximately 2 mm. The 1064 nm wavelength corresponds to an optical penetration depth that is much larger (80 mm) than the sample size, which should provide volumetric heating of the sample. The 1850 nm laser couples more strongly to water and thus has a smaller (0.8 mm) penetration depth. The 1850 nm laser can heat using a low laser power, but may not allow for uniform heating of the sample. There is minimal absorption of key subcellular components such as DNA and proteins at these wavelengths.[37]

This light-assisted drying technique has several advantages over drying methods that have been tested to date. The required equipment is relativity inexpensive making it appropriate for a wide range of applications. The system needed for light-assisted drying is scalable: it could be used on a small number of samples (e.g. clinical setting) or for industrial use (in-line processing). Thermal imaging allows for monitoring of the sample surface temperature during processing, which is not currently available for other techniques. Light-assisted drying also offers precise energy deposition into the samples that are being dehydrated. This is an important characteristic of this technique, as the energy deposition ultimately controls the drying rate and the end moisture content of the sample. The end moisture content drives many of the properties of the glassy state of the preservation matrix. In particular, the glass transition temperature is very sensitive to end moisture content, particularly at high glass transition temperatures/low end moisture contents. High glass transition temperatures are required for storage of the dried samples at supra-zero temperatures. This precision of energy delivery/end moisture content is not offered by other drying methods that have been used to date.

1.4   Droplet Drying

As mentioned previously, LAD will be used to form amorphous solids by increasing evaporation from 40 µl droplets of proteins suspended in a trehalose solution. To better understand the anhydrous preservation of a droplet of proteins it is beneficial to first consider the drying process of a basic water droplet under standard atmospheric conditions. Typically when a droplet is deposited on a substrate, such as borosilicate glass, it forms a spherical cap shape. Evaporation causes the volume of the drop to decrease. There are two types of evaporation modes; constant contact angle, where the radius of the droplet decreases over time, and constant contact area, where the contact angle decreases over time as shown in Figure 4. The latter will be used for the best approximation of our drying technique.
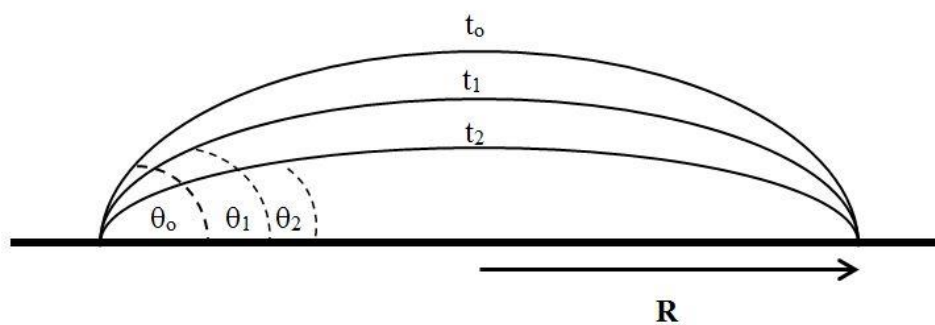
Figure 4: Constant contact area diagram of a droplet evaporating over time.

The drying rate of evaporation is governed by three main mechanisms. First, the phase change from liquid to vapor, in other words, the rate at which water molecules can cross the liquid-air border. As these molecules cross the interface, the air just above the

surface becomes saturated. This leads to the second mechanism that controls evaporation, the rate at which water vapor molecules are transported from the droplet surface into the surrounding medium, called diffusive transport. The third mechanism is heat transfer to the liquid-air interface which induces evaporative cooling. Water molecules near the surface boundary will evaporate if they have sufficient kinetic energy to overcome liquid phase intermolecular forces. As these higher kinetic energy molecules escape, the remaining molecules have a lower kinetic energy. Since temperature is proportional to kinetic energy this means the droplet temperature will decrease.[38]

The rate of volume change, evaporative flux, can be used to determine the lifetime of a droplet. Evaporative flux can be estimated using some simplifying approximations. Assume the droplet volume, V, is proportional to the cube of the droplet radius, R, and that the diffusion time of water vapor is given by

$$t_d = \frac{R^2}{D} \qquad \text{[Equation 3]}$$

where D is the diffusion constant for water vapor in air. These relationships can be combined to give the rate at which the volume decreases over time

$$\frac{dV}{dt} \sim -\frac{R^3}{t_d} = -DR \qquad \text{[Equation 4]}$$

A Marangoni stress (surface-tension gradient) will develop in a sessile drying droplet because of the thermal gradient across it arising from evaporative cooling. This drives a recirculating flow within the droplet.[39] In our technique we have control over the lateral thermal gradient of our sample, which could lead to higher drying rates. Using a standard water-only droplet is effective for explaining evaporative rates during LAD processing, but it should be noted that the actual preservation solution contains trehalose molecules that will cause the sample to become increasingly viscous as it dries.[40]

1.5   This Project

This dissertation describes the development of the LAD process (Chapter 2), the characterization of LAD processed and stored samples (Chapter 3), and the testing of protein functionality of proteins preserved with LAD (Chapter 4). Chapter 2 details the drying capabilities of LAD and optimization of processing parameters including laser wavelength, power, and sample substrate. Chapter 3 covers the optical characterization of LAD samples using polarized light imaging (PLI), scanning white light interferometry (SWLI), and Raman spectroscopy. Polarized light can be used to image crystal structures. SWLI is widely used for optical profiling and generates a height map across the sample that we can use to determine sample topography.[41],[42] Raman spectroscopy measures the frequency shift of inelastic scattered light. This technique is used for monitoring trehalose distribution. Finally, Chapter 4 tests the actual application of LAD on an immobilized model protein, lysozyme, to determine protein functionality post processing and after short term storage.

CHAPTER 2: EMC STUDIES AND LAD OPTIMIZATION

2.1   Introduction

In this study, we use a new technique, light-assisted drying (LAD), to form an amorphous trehalose solid. LAD uses illumination by NIR laser light to assist in the formation of trehalose amorphous solids. Static air-drying of sugar solutions is dominated by evaporative cooling which causes the drying rate to slow substantially and allows for crystallization of the sugars. LAD selectively heats water to overcome cooling due to evaporation and accelerates dehydration of the samples. Two laser sources at 1064 nm and 1850 nm wavelengths were used to heat water in small volume samples. There is minimal absorption of key subcellular components such as DNA and proteins at these wavelengths.[37] In this paper, the water content of trehalose glasses formed via LAD using different laser wavelengths (1064 nm and 1850 nm), laser powers and processing times as well as their thermal histories during processing are presented. Two wavelengths with different absorption coefficients in water were chosen to test the effect of optical penetration depth in the sample on their resultant EMC. In addition, two drying substrates - borosilicate glass cover slips and a microfiber filter paper – were tested. Predicted glass transition temperatures for the trehalose preservation matrices produced via LAD are calculated and discussed.

2.2   Methods

A schematic of the experimental setup is shown in Figure 5. Two IPG Photonics laser sources were used separately for LAD processing, a continuous wave (CW) ytterbium fiber laser at 1064 nm (YLR-5-1064) and a CW thulium fiber laser at 1850 nm (TLM-5).
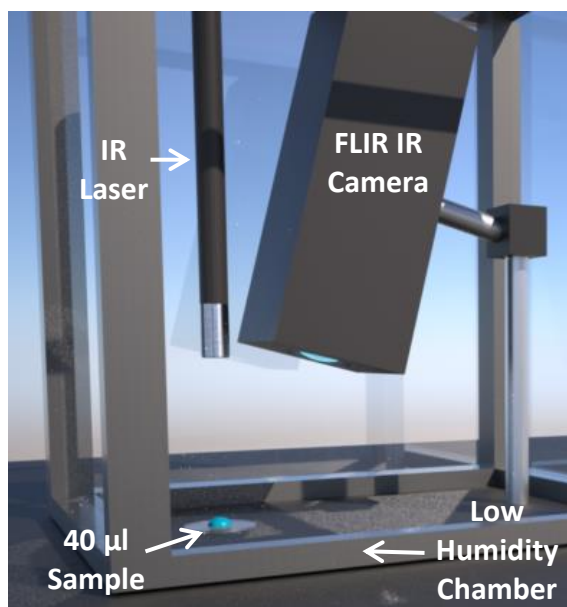
Figure 5: Experimental set-up of light-assisted drying (LAD) technique within a controlled low relative humidity chamber.

Both sources have maximum power outputs of 5 W with built in control of power and current, respectively. Both lasers emit collimated, single-mode, Gaussian beams with a FWHM spot sizes of ~4.5 mm which were measured using a BeamTrack 10A-PPS thermal sensor (Ophir Photonics). A FLIR SC655 mid-IR camera was used to record the temperature of samples in all tests. The camera has an array of 640x480pixels and a maximum frame rate of 200 fps. This camera is sensitive from 7.5 to 14 microns, which

is ideal for sensing temperature in the ranges that we are studying (35°C - 77°C). All studies were performed in a humidity-controlled environment that was kept at approximately 11% relative humidity (RH). This was achieved by pumping dried air into a chamber containing the experimental setup and monitoring the RH with a temperature and RH logger (ONSET UX100-011). Maintaining a low relative humidity expedited the drying process.

All samples in the studies consisted of 40µl droplets containing a model protein, egg white lysozyme (Worthington Biochemical LS002933), dissolved in drying solution (DS) at a concentration of 0.5 mg/ml. This was verified using the absorption of light at 280 nm with a microplate spectrophotometer (Bio-Tek Synergy HT). The DS consisted of 0.2M disaccharide trehalose in 0.33 x phosphate buffer solution (PBS).[43] The dry weight of DS was determined through bake out method to be 7.01% the mass of a sample. Dry weight was adjusted to include the mass of the protein based on its concentration to determine the total dry weight.

For each test, a 40 µL droplet of the protein/drying solution was deposited onto a substrate and the initial mass was determined gravimetrically using a balance (RADWAG AS 82/220.R2) accurate to 0.01mg. The sample was then moved into the humidity chamber for laser irradiation. The temperature of the sample was monitored during processing using the thermal camera. Maximum sample temperature was recorded as a function of time for each sample. After irradiation, the sample was removed from the humidity chamber and immediately massed again. End moisture content (EMC), which is a measure of the amount of water relative to the dry mass of a sample, was calculated as:

$$EMC = \frac{m_f - m_s - m_{dw}}{m_{dw}} \qquad \text{[Equation 5]}$$

where m_f is the mass of the final sample including the mass of the substrate, m_s, and m_{dw} is the calculated dry weight of the initial sample.

Several different sets of processing parameters were tested and EMC as a function of LAD processing time (0 – 60 min) was determined (see Table 2). Each experiment was repeated three times (N=3), with the exception of the 1064 nm laser at $T_{max} = 43.0 \pm 1.8°C$ on coverslips at 30 and 60 minutes of processing (N=20) to test EMC repeatability. In addition, identical samples were allowed to air dry in the relative humidity chamber as a control.

Table 2: Processing parameters tested for LAD drying. Wavelength, power, and substrate were varied.

1850 nm	Beam Size (mm)	Power Density (W/cm^2)	Processing Power (W)	T_{max} (°C)
	4.009	0.88	0.11	35.0±2.4
Coverslip	4.009	1.42	0.18	42.4±2.1
	4.009	4.04	0.51	77.6±1.2
	24.054	0.18	0.86	36.4±0.9
Filter Paper	24.054	0.29	1.36	43.9±0.7
	24.054	1.01	4.60	72.5±0.3

1064 nm	Beam Size (mm)	Power Density (W/cm^2)	Processing Power (W)	T_{max} (°C)
Coverslip	4.864	16.15	3.00	35.2±0.9
	4.864	26.92	5.00	43.0±1.8

For the 1850 nm laser source, three laser powers were tested with each resulting in a different maximum temperature of the sample during processing. We chose to test

various laser powers to determine the effect of processing temperature on drying rate. Two different substrates were tested using the 1850 nm laser - 18mm diameter borosilicate glass coverslips (Fisherbrand 12-546) and 8 mm diameter borosilicate glass microfiber filter paper (Whatman 1821-021). The glass cover slips allow for easy recovery and rehydration of the proteins, while the filter paper is used in diagnostic assays. On the glass coverslips, the samples were droplets approximately 2 mm in thickness with a diameter of approximately 7 mm. A 1.0 ND filter (Newport 5214-A) was placed in line with the 1850 nm laser for processing samples on coverslips since the lowest available power setting caused excessive heating. On the filter paper, the samples dispersed in the paper such that they were a constant thickness of 0.675 mm, with diameter 8 mm. Filter paper samples have a constant sample thickness in comparison to their droplet counterparts so the Gaussian beams had to be flattened to allow for even heating across the samples. The 1850nm laser beam was "flattened" using a reflective 6X beam expander (Thorlabs BE06R). Samples were placed in the middle of the expanded beam where there was minimal change in beam profile.

With the 1064 nm laser, two different laser powers were used for processing. Due to the lower absorption coefficient of water at 1064 nm, we were not able to achieve sample temperatures above about 42°C even at the maximum power output of the laser. In addition, only glass coverslips were used as the substrate for these tests. Beam shaping the 1064 nm did not give a high enough energy density to achieve necessary processing temperatures to process filter paper samples.

2.3   Results & Analysis

Drying curves summarizing the results are shown in Figure 6. Drying curves are graphs of EMC versus processing time and allow easy comparison of the EMC resulting from different sets of processing parameters.
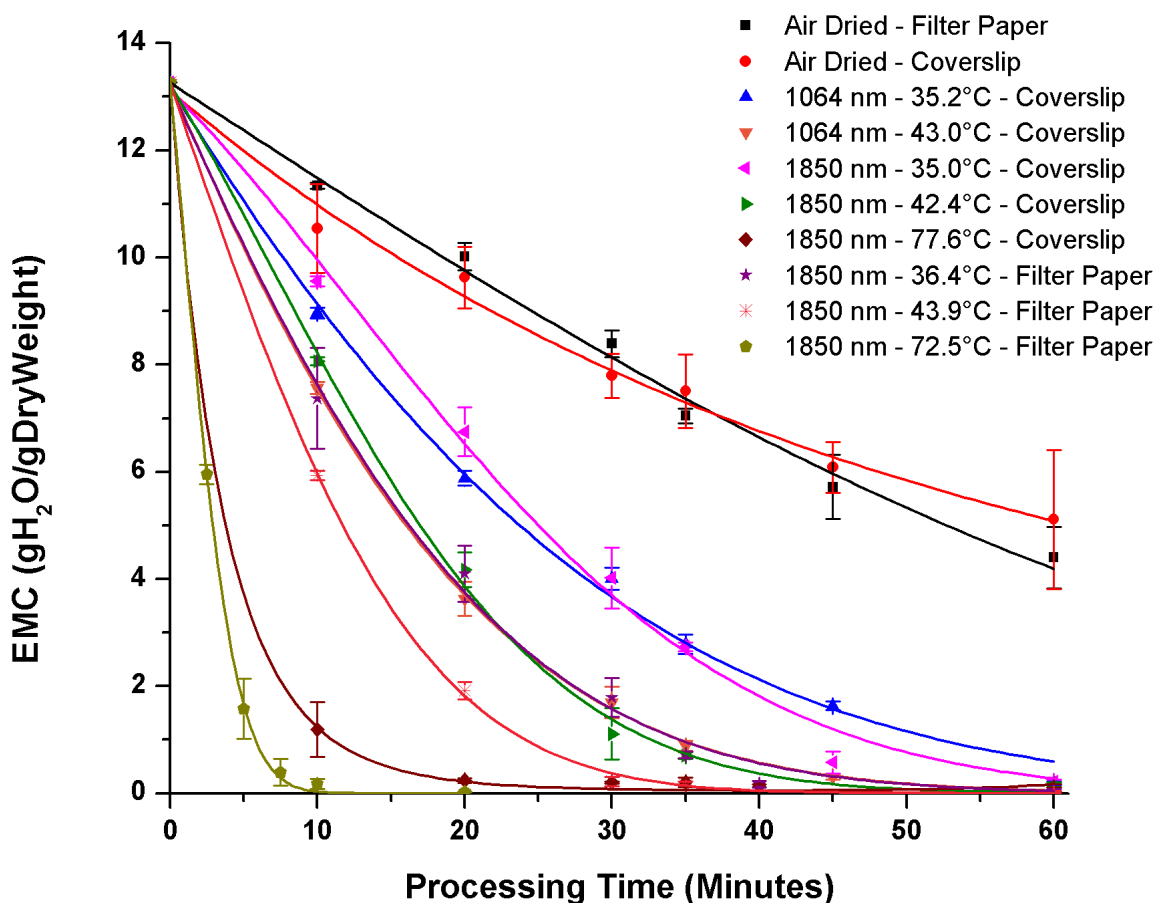
Figure 6: EMC as a function of processing time for various processing

Table 3 summarizes the resulting EMC, sample temperatures and predicted glass transition temperatures for 60 minute processing times for both lasers and for air drying. Air drying resulted in much slower drying and much larger EMC's at all processing times than either laser source. During air drying evaporation reduces the temperature of the

sample and this decreases the evaporation rate. With light assisted drying, the laser adds energy to the drop to counteract/slow the effects of evaporative cooling.

Table 3: EMC for each set of processing parameters and their associated glass transition temperatures.

Wavelength (nm)	Substrate	T_{max} (°C)	T_p (minutes)	EMC ($gH_2O/gDryWeight$)	T_g (°C)
1850	Coverslip	35.0±2.4	60	0.22±0.04	-25.4
		42.4±2.1	60	0.16±0.04	-6.7
		77.6±1.2	60	0.14±0.03	1.0
	Filter Paper	36.4±0.9	60	0.06±0.03	44.1
		43.9±0.7	60	0.03±0.02	68.3
		72.5±0.3	20	0.03±0.01	68.3
1064	Coverslip	43.0±1.8	60	0.17±0.04	-10.3
		35.2±0.9	60	0.19±0.03	-16.8
Air Drying	Coverslip	N/A	60	5.11±1.3	-126.5
	Filter Paper	N/A	60	4.40±0.6	-125.2

We tested two laser wavelengths in this study, 1064 nm and 1850 nm, and compared the drying capabilities of these two wavelengths for drops deposited on the glass coverslip substrate. To compare the resulting drying curves for these two wavelengths, we compared laser powers that resulted in the same maximum sample temperatures during processing. The temperatures were measured using the thermal camera. We compare the performance of the lasers at maximum sample temperatures of 35°C and 42°C. For both lasers, as the maximum sample temperature increased from 35 °C to 42 °C, the resulting EMC after 60 minutes is lower, as expected. The EMCs at 60 minutes for both laser sources were approximately the same. With the temperature of the drops being approximately the same, similar evaporation rates are expected. The power density used with the 1850 nm laser was much lower than that of the 1064 nm laser. This

is because the water absorption coefficient for the 1850 nm laser is much higher than the 1064 nm laser. Therefore, even with less power per unit area, the sample heated at a similar rate due to more of that power being absorbed by the water. We then tested an additional temperature, 77°C with the 1850 nm laser, and saw an even further decrease of EMC. Overall we see that both lasers have similar drying curves at the same processing temperature. The 1850 nm laser yields the lowest EMC but at the cost of a higher processing temperature. The low power needed to achieve this drying is an advantage but could also mean uneven sample heating because of the short penetration depth.

Looking at the drying curves in detail (see Figure 7) reveals an interesting result when comparing drying curves for each wavelength at similar processing temperatures.
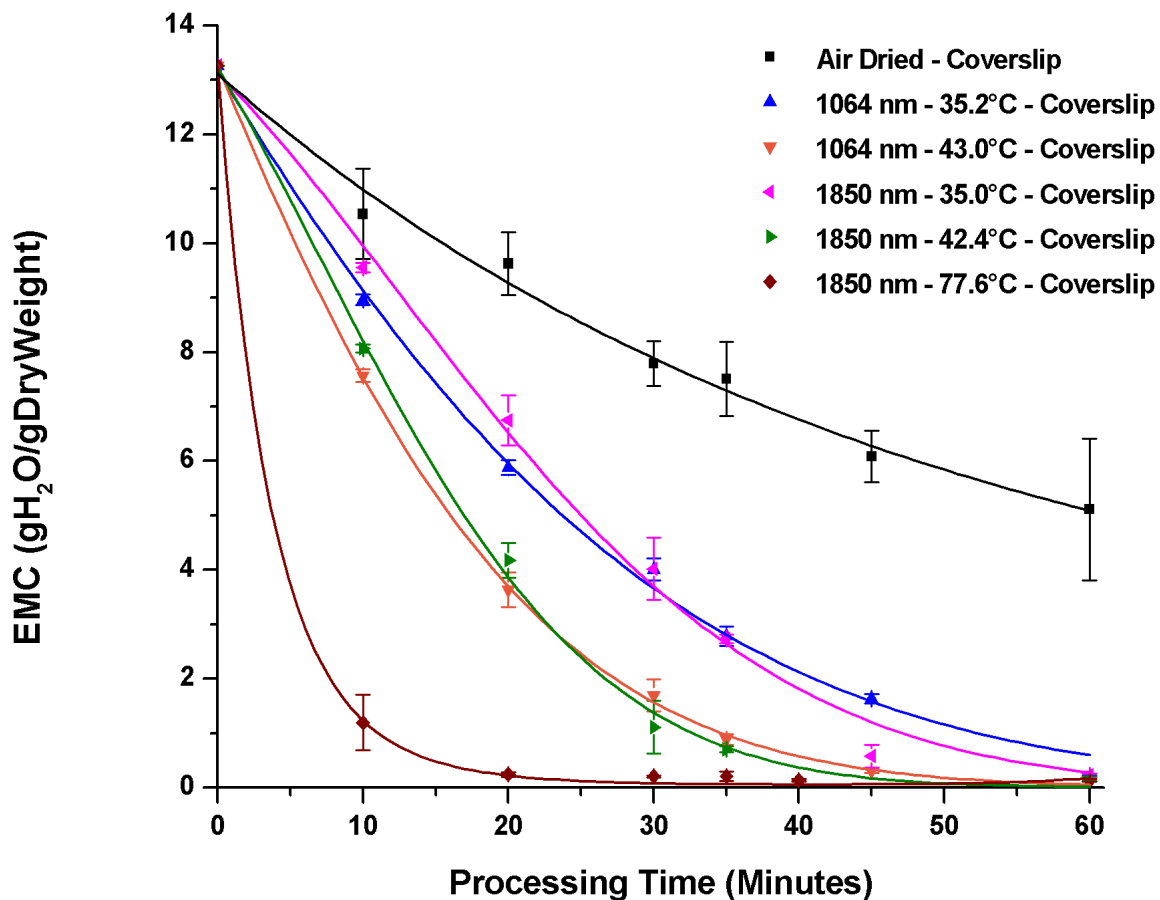
Figure 7: EMC as a function of processing time for drying on coverslips.

For short processing times (<30 minutes) the 1064 nm laser provides lower EMCs, but for processing times greater than 30 minutes the 1850 nm laser results in lower EMC until the drying curves converge at 60 minutes. This happens at both low and intermediate laser powers (35°C and 42 °C sample temperatures). Also, the slope of the drying curve, which indicates the drying rate, is initially steeper for the 1064 nm laser, but after 30 minutes of processing time the drying rate of the 1850 nm laser is steeper. The absorption coefficient for the 1850 nm laser source may account for these differences in the drying curves. Initially, 1064 nm light couples effectively because there is more

water to interact with. As the water evaporates, the 1064 nm source couples less strongly causing the amount of energy deposited to decrease, and subsequently the slope of the drying curve flattens. A possible method to combat this issue is to increase the power of the 1064 nm source during processing.

Recall the N=20 for the 1064 nm laser at ~43.0°C at processing times of 30 and 60 minutes. Increasing the sample size from N=3 to N=20 we saw a slight increase in average EMC and standard deviation at 30 minutes by 0.28±0.19 $gH_2O/gDryWeight$ and a slight decrease at 60 minutes by 0.02±0.37 $gH_2O/gDryWeight$. This implies that LAD has better repeatability at low EMCs.

We tested two substrates – glass coverslips and filter paper – with the 1850 nm laser (see Figure 8 and Table 3) at sample temperatures of 35°C and 42°C.
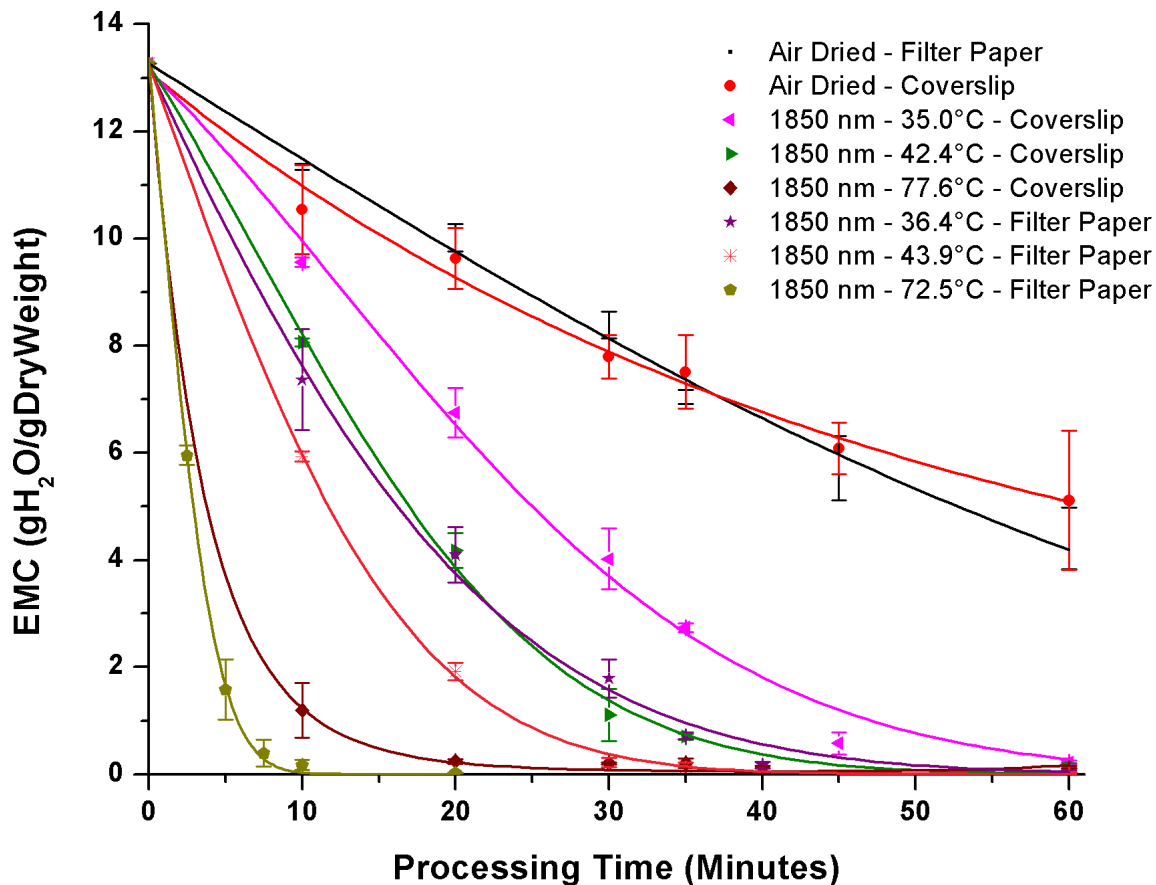
Figure 8: EMC as a function of processing time for drying with 1850 nm laser.

Drying on the glass coverslips was slower than drying on the filter paper (for comparable sample temperatures); filter paper gave the lowest EMC. This is likely the result of the difference in surface tension of the sample on coverslips versus filter paper. On the coverslips, the sample maintains a hemispherical droplet shape, while on the filter paper the drop spreads out and assumes a 2D planer structure. The surface tension of the droplets on coverslips decreases the evaporation rate. The filter paper breaks up the droplet and spreads out so it is thinner, increasing surface area and reducing the surface tension. We tested the 1850 nm laser source of the filter paper at a higher power that

resulted in a maximum sample temperature of 72°C. At the high temperature, the EMC at 20 minutes was comparable to 60 minutes of processing at a temperature of 36°C on filter paper.

All light-assisted processing provided EMCs with good repeatability as measured by the small standard deviation of the mean at all processing times and for all laser parameters (see Table 3). This was not the case for air drying which had a very high variability in EMC. The repeatability of light-assisted drying is likely due to precise and repeatable energy deposition into the samples during processing.

The maximum sample temperature was recorded during processing for each sample to give thermal history. The average maximum sample temperature for the 60 minute samples was averaged for an N=3 thermal history. In Figure 9 we compare the EMC to the corresponding thermal history for each set of processing parameters at similar processing temperatures.
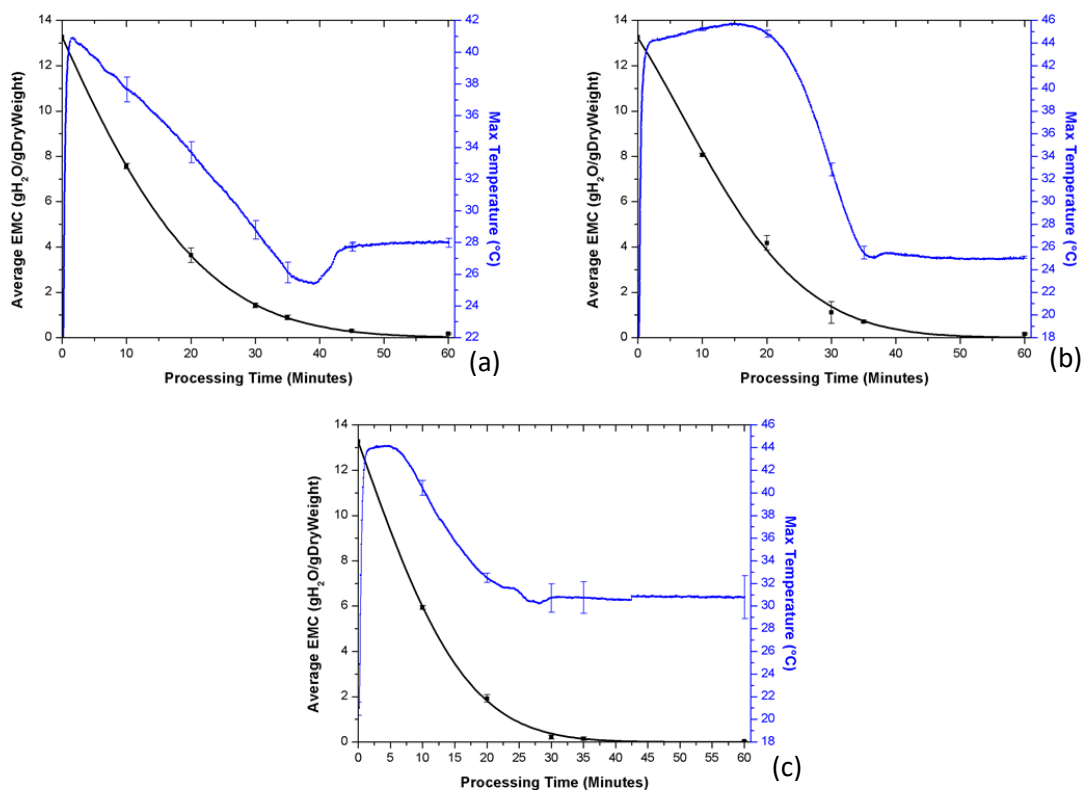
Figure 9: Thermal histories with EMC curves for LAD processing of (a) 1064 nm on coverslips, (b) 1850 nm on coverslips, and (c) 1850 nm processing on filter paper for similar processing temperatures.

In all cases there is initial heating of the drop as the laser energy is added. Once evaporation begins cooling occurs. All samples experience this cooling effect during processing but at different times. Evaporative cooling is removing more energy than the laser adds through absorption. As the sample evaporates the laser couples less strongly. To overcome evaporative cooling we would need to increase laser power.

Maximum sample temperature for the 1064nm on coverslips did not maintain peak temperature throughout processing, evaporative cooling was the dominate mechanism and the sample cooled until approximately 40 minutes of processing. The

1064nm laser coupled less strongly with the water and its maximum power did not deliver sufficient energy to overcome evaporative cooling. Heating resumed again and plateaued at 28°C, most likely due to heating of the coverslip. Figure 10 shows the heating of a glass coverslip with the 1064 nm laser at 5W. We see the same characteristic plateau that is observed at the end of the samples thermal histories.
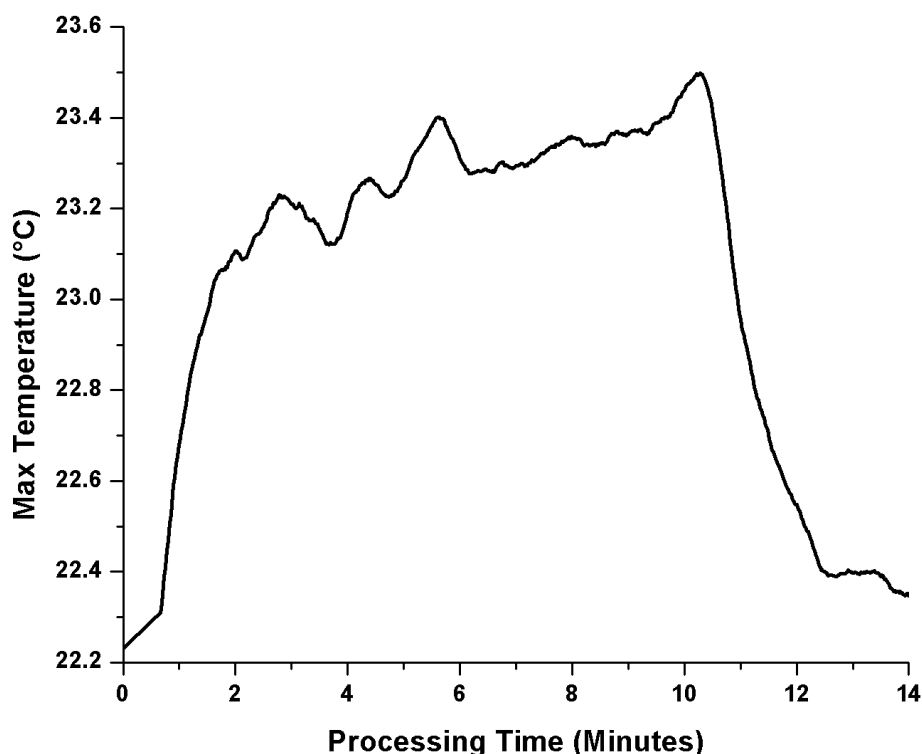
Figure 10: Thermal history of borosilicate glass coverslip without sample under illumination with 1064 nm laser at 5 W. This is the same processing parameters associated with Figure 6 (a). This heating curve corresponds to the heating observed during the end of LAD processing after most of the water has been removed from the sample.

Maximum temperature for the 1850 nm laser on coverslips showed an increase in sample temperature for the first 20 minutes because it coupled more strongly with water

in the sample and delivered sufficient energy to overcome evaporative cooling. At ~20 minutes the volume of water had decreased, therefore less energy was being delivered and evaporation caused a drop in temperature. After 35 minutes of processing we saw a small increase in temperature followed by a plateau at 25°C caused by the heating of the coverslip.

Finally, maximum sample temperature for the 1850 nm laser on filter paper showed the same increase in sample temperature followed by a decrease from evaporative cooling and a small increase from substrate heating that was observed in the thermal history of 1850 nm coverslip drying but on a shorter timescale. Also note that the substrate heating of the filter paper plateaus at a higher temperature than the coverslip. This is likely because the filter paper fibers scatter the incoming light increasing the optical path length of the light in the substrate and allowing for more absorption.

For all LAD drying, the point at which substrate heating took effect was at an EMC = 0.58 ± 0.04 gH$_2$O/gDryWeight. This was because the volume of water left in the sample was low enough that there was negligible water absorption and laser energy was absorbed by the substrate.

2.4   Disussion

Both the 1064 nm and 1850 nm laser sources show promise for use in the preparation of trehalose glasses to be used for the preservation of proteins or other biologics. Table 3 shows the predicted storage temperatures (T$_g$) for the samples prepared in this study. The estimated T$_g$ for drops dried on coverslips are close to 0 °C. This is an improvement compared to the sub-zero storage temperatures required for some proteins, but on par with lyophilized proteins that require cold chain storage. Finally, the samples

did not reach sufficiently low EMC that would have a T_g near room temperature. There are multiple ways to improve this result. Longer processing time is one option; however, with the drying curves flattening out substantially at processing times of 60 minutes, the additional drying observed past this point would likely be small. Adding more power would increase the sample temperature and would therefore increase the drying. With this solution comes the risk of damaging the embedded protein. Finally, we could add a surfactant to the solution to decrease surface tension, which would increase the drying rate.

The standard deviation of the technique is low compared to air drying, however future studies will take a closer look at repeatability, as slight variations at very low EMC can lead to large variations in T_g. It should be noted that gravimetrically determining EMC is only an indicator of the average EMC of the entire sample. This does not show the varying moisture contents across the sample, which would lead to a higher storage temperature that corresponds to the area of highest EMC.

The combination of the 1850 nm source and the filter paper substrate provided the best results. The predicted storage temperatures for the samples processed on filter paper are promising for storage at ambient temperatures. For example, after 60 minutes of processing the 1850 nm laser produced trehalose glasses with potential storage temperatures ranging from 47°C-69°C. Light-assisted drying on filter paper is appropriate for use in diagnostic assays but not for protein therapeutics where biocompatibility of filter particulates needs to be considered.

Freeze drying can take multiple hours to complete. A LAD processing time of an hour is a considerable improvements. Light-assisted drying (LAD) offers a relatively

inexpensive, compact method for initial processing and anhydrous preservation allows for low-maintenance storage after samples have been packaged. LAD has the potential to provide a processing and storage method for protein-based drugs and diagnostic assays by forming an amorphous material around the proteins that will maintain their structural conformation, while increasing shelf life by decreasing bioactivity.

CHAPTER 3: OPTICAL CHARACTERIZATION OF LAD SAMPLES

3.1   Introduction

This chapter discusses the optical characterization of LAD samples after processing using polarized light imaging (PLI), scanning white light interferometry (SWLI), and Raman spectroscopy.

PLI is used to measure the homogeneity of amorphous materials and locate areas of crystallization. We looked for crystallization immediately post LAD processing and also monitored the crystallization kinetics of the same samples stored in three different relative humidity (RH) environments. Localized areas of crystallization in the samples can act as nucleation points and increase the rate of crystallization as well as lead to physical stress on some biologics embedded in the matrix.[44] Polarized light microscopy has been used previously to analyze the presence of crystallization in sugars.[45] When light passes through a linear polarizer it only transmits the component of the electric field that is in the direction of the transmission axis producing linearly polarized light. When that light passes through a secondary linear polarizer (analyzer) with a transmission axis oriented perpendicular to the first polarizer the light is completely absorbed. This is referred to as crossed polarizers. When a crystal is placed between a pair of crossed polarizers its optical anisotropy will cause the polarization state of linear light passing through it to rotate. Depending on the amount of rotation a component of the electric field will pass through the analyzer allowing it to be detected. In contrast, when an optically

isotropic material, such as glass, is placed between crossed polarizers it will not undergo any change in polarization state and will not pass through the analyzer. This allows us to image crystals that might be present in amorphous trehalose glass.

Scanning white light interferometry (SWLI) is used to measure sample thickness and surface morphology after LAD processing and after long term (~1 month) storage at low RH. In a Michaelson interferometric objective, white light is amplitude split into a fixed length reference beam and a measurement beam whose coherence plane matches the focal plane of the objective. Vertically scanning the measurement beam generates fringes as the coherence plane reflects off of the sample surface. The height value for each pixel across the sample corresponds to the z location of maximum fringe visibility. Variations in thickness across the sample may indicate an uneven distribution of the trehalose preservation matrix which could impact the overall functionality of embedded proteins.

Raman spectroscopy is used in conjunction with SWLI to investigate trehalose distribution across LAD processed samples. Photons incident on a molecule are predominately Rayleigh scattered (elastically scattered), and the energy of outgoing photons is equal to incoming photons. An electric field incident on a molecule induces a dipole moment that scatters light at the optical frequency of the incident wave. Molecular vibrations alter the polarizability of the molecule causing the incident photon to either lose energy by exciting the molecule to a higher vibrational state (Stokes shift) or gain energy by from a vibrationally excited molecule (anti-Stokes shift). This emitted light is a lower frequency or higher frequency than the incident light, respectively. Stokes shifted scattering is the predominate type of spectra because the thermal population of

vibrational excited states are typically low in ambient environments. Raman shift spectra depend on the atoms comprising the molecule as well as their atomic arrangements. This makes it ideal for determining the unique spectra of various chemicals.[46],[47]

3.2   Methods

3.2.1   LAD Processing & Sample Solution

The LAD system with the 1064 nm laser (as described in Chapter 1) was used for processing. Samples were processed for 60 minutes at 5W (26.9 W/cm^2). For each test, a 40 μL droplet of the protein/drying solution as previously discussed was deposited onto an 18mm diameter borosilicate glass coverslip (12-546, Fisherbrand) substrate and the initial mass was determined gravimetrically using a 0.01mg readability balance (AS 82/220.R2, RADWAG). A fiducial was marked on the edge of the coverslip to ensure consistent orientation for each measurement. The sample was then moved into the humidity chamber for laser irradiation. After irradiation, the sample was removed from the humidity chamber and immediately massed again and EMC was calculated.

3.2.2   Sample Storage Conditions

All samples were stored individually in small volume containers above a saturated salt solution of lithium chloride (LiCl) (ChemCenter) and tested at various storage times (t_s). The RH of the LiCl saturated salt was 14.3±0.5 RH. This was measured with an RH probe (HH314A, Omega) in a separate container for the duration of the samples storage. The PLI study also included two other sets of storage RH for testing: potassium acetate (KOAc) and magnesium nitrate ($Mg(NO_3)_2$) (Carolina Biological) at 24.2±1.9% RH and 47.2±5.8% RH respectively.

3.2.3 Polarized Light Imaging

The PLI experimental set-up (Figure 11) consisted of a white light fiber optic illuminator (41720, Cole Palmer), two linear polarizers (LPVISE050-A, Thorlabs), with the second polarizer acting as an analyzer, and a digital camera (Nikon D100) aligned in the vertical direction. The camera was equipped with a Nikon 28-105mm f/3.5-4.5 lens and manually focused on the image plane. The spatial resolution of the set-up was 10μm/pixel. LAD samples (N=8) were processed as described in Section 3.2.1 and air dried samples (N=4) were made at the same time as LAD samples by drying at low RH (~14% RH) for 60 minutes. Samples were placed in between the polarizers on a glass microscope slide and imaged from above. Two images were taken: the first with the analyzer oriented at 0° to the polarizer and the second with the analyzer oriented at 90° to the polarizer. Samples were imaged and massed immediately after LAD processing then placed in low RH containers previously mentioned. They were then imaged and massed every 30 minutes for the first two hours in storage, then every hour for the next 2 to 5 hours and once a day after that.
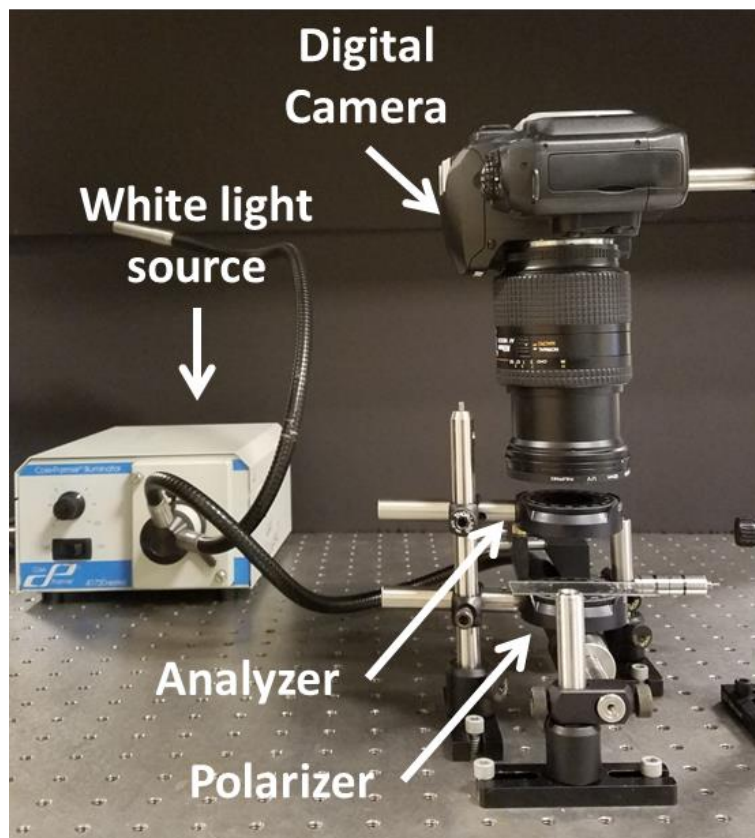
Figure 11: Polarized light imaging set-up. Samples were placed on a borosilicate glass coverslip between the polarizer and analyzer.

3.2.4 Scanning White Light Interferometry

Sample thickness was measured with a Zygo Nexview Scanning White Light Interferometer (SWLI) with a 2.75X Michelson objective (spatial resolution: 5.88 µm/pixel). Samples (N=7) were LAD processed as previously mentioned and stored in LiCl (14.3±0.5% RH) containers and measured after one day of storage and again after 27 days of storage. EMC was measured just prior to all SWLI measurements. The data was exported into Matlab and HDFView for further processing. In Matlab transverse height was displayed as a color map across the sample, the average maximum height of

the sample was calculated, and two diagonal cross sections were extracted. The HFView

software was used to extract the non-interferometric images.

3.2.5 Raman Spectroscopy

Raman spectroscopy was used to measure the Raman shift of trehalose across

LAD processed samples. A schematic of the Raman spectroscopy set-up is shown in

Figure 12.
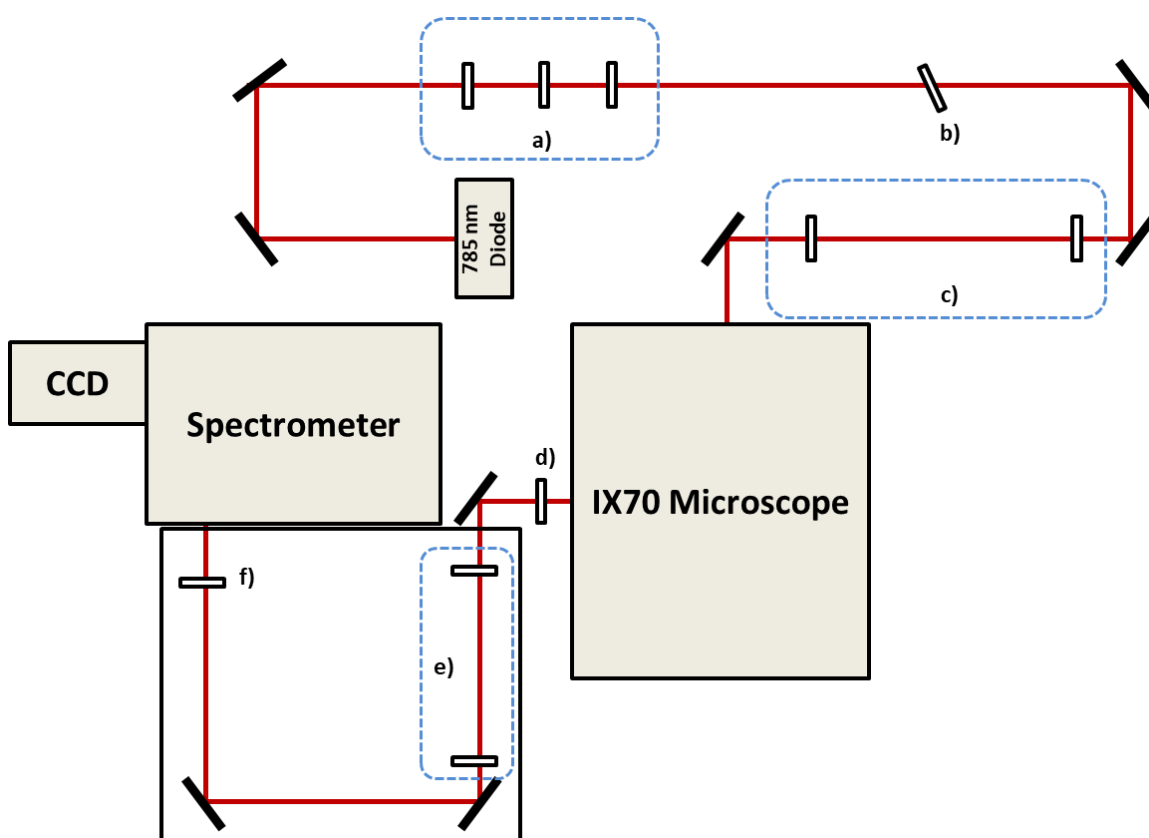
Figure 12: Raman spectroscopy set-up. The laser beam passes through a) a lens system
with a 100 μm pinhole to clean up the intensity profile followed by a b) 785 nm notch
filter to spectrally clean up the beam and then an c) expander into the microscope. The
Raman signal from the sample exits the microscope and passes through an d) edge filter
to remove the excitation wavelength. Then it goes through a e) beam expander and
collimator before passing through a f) focusing lens into the spectrometer.

The excitation source was a 785 nm laser diode (BeamQ) with a power output of 200 mW, the beam passed through a 100 µm pinhole and 785 notch filter to spatially and spectrally clean up the beam. The beam was then expanded and collimated before entering an IX70 inverted microscope (Olympus). A 100X oil immersion objective was used to focus the light onto the sample. Raman signal from the sample was then collected back into the objective lens and directed into a spectrometer (SR-303i-B, Andor) and imaged with a CCD camera (DU420A-BR-DD, Andor) with a spectral resolution of 0.28 nm/pixel. The spectrometers center wavelength was set to 855.36 nm to exclude the laser line from the spectra and signals were taken at an exposure time of 5 seconds and 60 accumulations to achieve maximum signal to noise ratio.

Samples (N=5) were LAD processed and EMC was measured as previously mentioned followed by storage in LiCl (14.3±0.5% RH) containers. After one day of storage EMC was measured and SWLI was performed as described above. The following day the Raman shift spectra were taken at three separate locations across each sample. Each spectrum was background corrected and baseline corrected to remove the signal from the coverslip using Andor Solis software. Corrected spectra were exported to Matlab where they were Savitzy-Golay smoothed and then normalized to their maximum.

3.3   Results & Analysis

3.3.1   PLI & Effect of Storage RH on EMC

For each set of RH EMC as a function of storage time was plotted. Figure 13

shows the change in EMC as a function of storage time for LAD processed and air dried
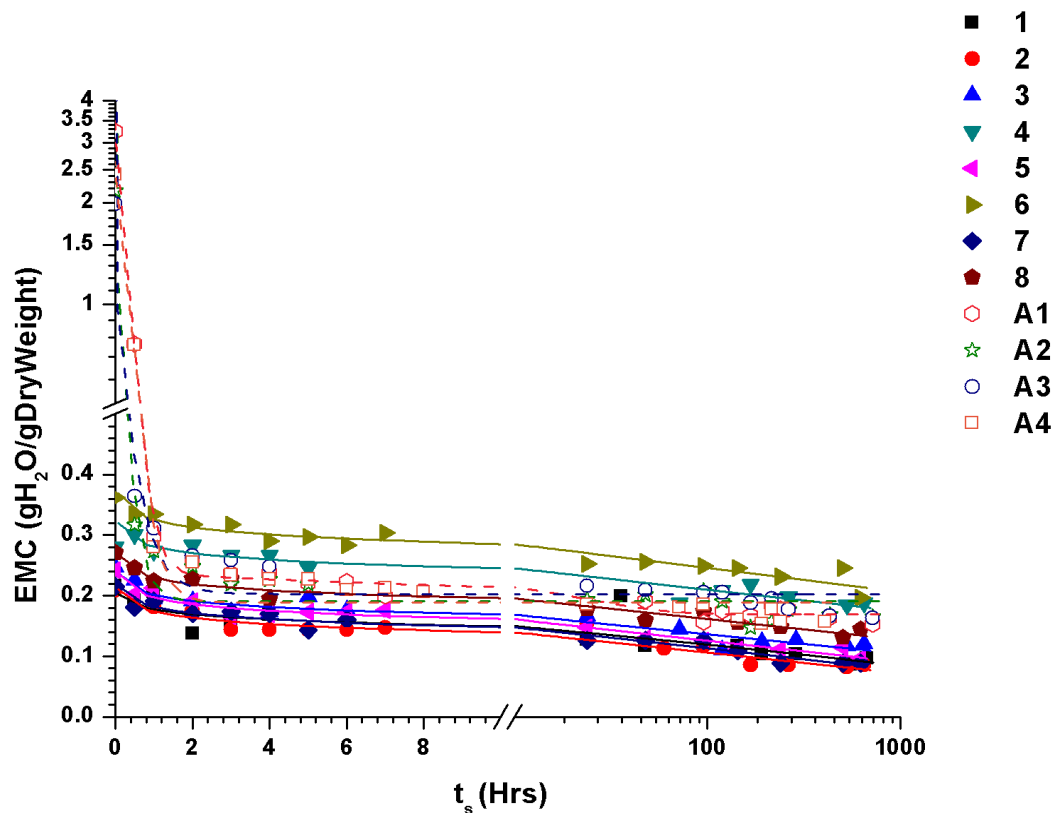
Figure 13: EMC as a function of storage time for air dried (A1-A4: exponential decay fit) and LAD (1-8: power fit) processed samples stored at 14.3±0.5% RH.

samples. All air dried samples showed an exponential decrease in moisture content with

the highest evaporation rate occurring during the first 3 hours and reached a moisture

loss limit after 10 hours. After approximately 100 hours of storage samples approached

their moisture loss limit which corresponded to the halt in crystal growth.

The second set of samples was stored at 24.2±1.9% RH. Figure 14 shows EMC as a function of storage time for air dried and LAD processed samples stored at 24.2±1.9% RH. Air dried samples experienced an exponential decrease in EMC within 3 hours to within the same EMC area as the LAD processed sample. LAD samples experienced a nonlinear decrease in EMC over storage time with the largest drop in EMC occurring within the first 10 hours.
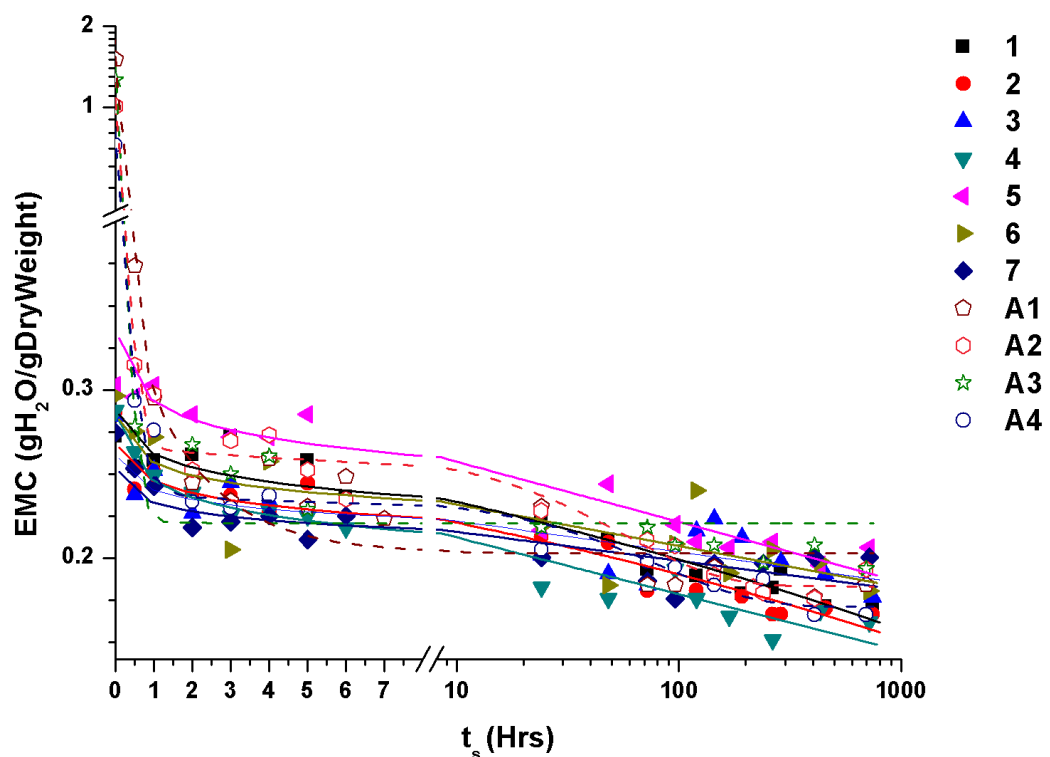
Figure 14: EMC as a function of storage time for air dried (A1-A4: exponential decay fit) LAD (1-7: power fit) processed samples stored at 24.2±1.9% RH.

The final set of samples was stored at 47.2±5.8% RH. Figure 15 shows the EMC of air dried and LAD samples during storage. Air dried samples highest rate of crystallization and highest rate of evaporation both occurred within 2 hours of storage.

LAD samples experienced a linear decrease in EMC during storage after 10 hours. Sample 3 did not experience any decrease in EMC during storage.
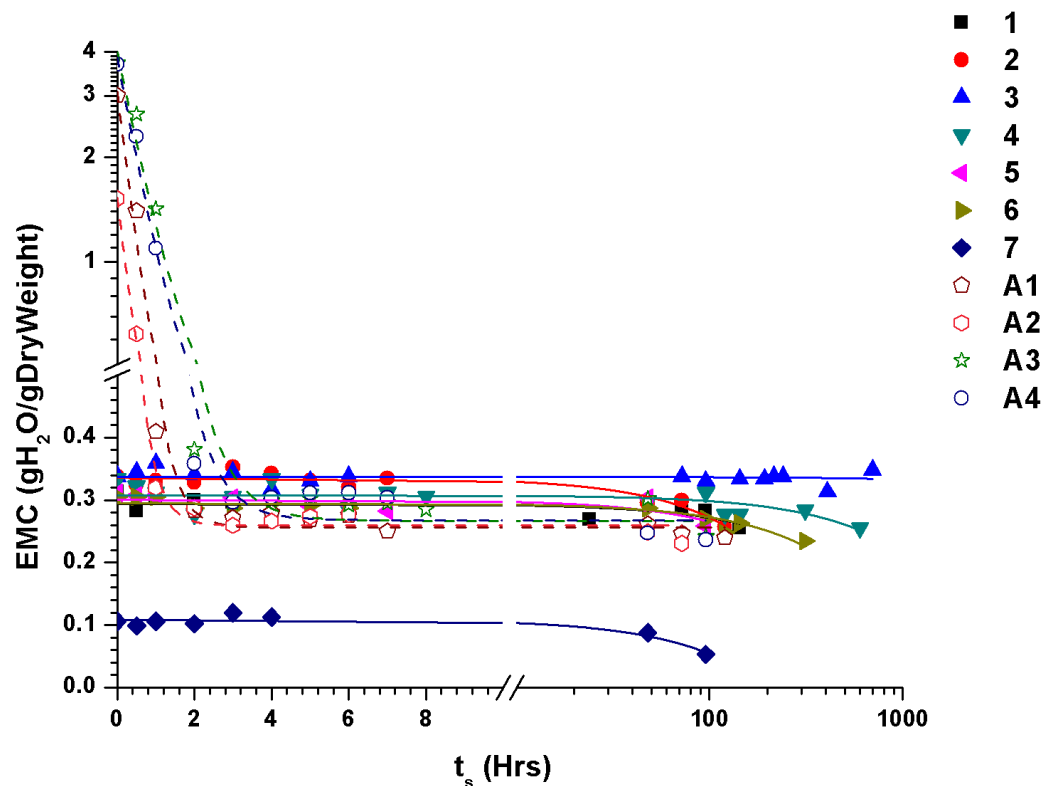
Figure 15: EMC as a function of storage time for air dried (A1-A4: exponential decay fit) and LAD (1-7: linear fit) processed samples stored at 47.2±5.8% RH.

Figure 16 shows EMC as a function of storage time for each set of RH. We see that the 14.3±0.5% RH generally yielded the lowest EMC over time. This is beneficial for achieving a higher glass transition temperature so we chose this as the storage RH for all future studies. Cracking observed near the end of storage at this RH is discussed in the next section.
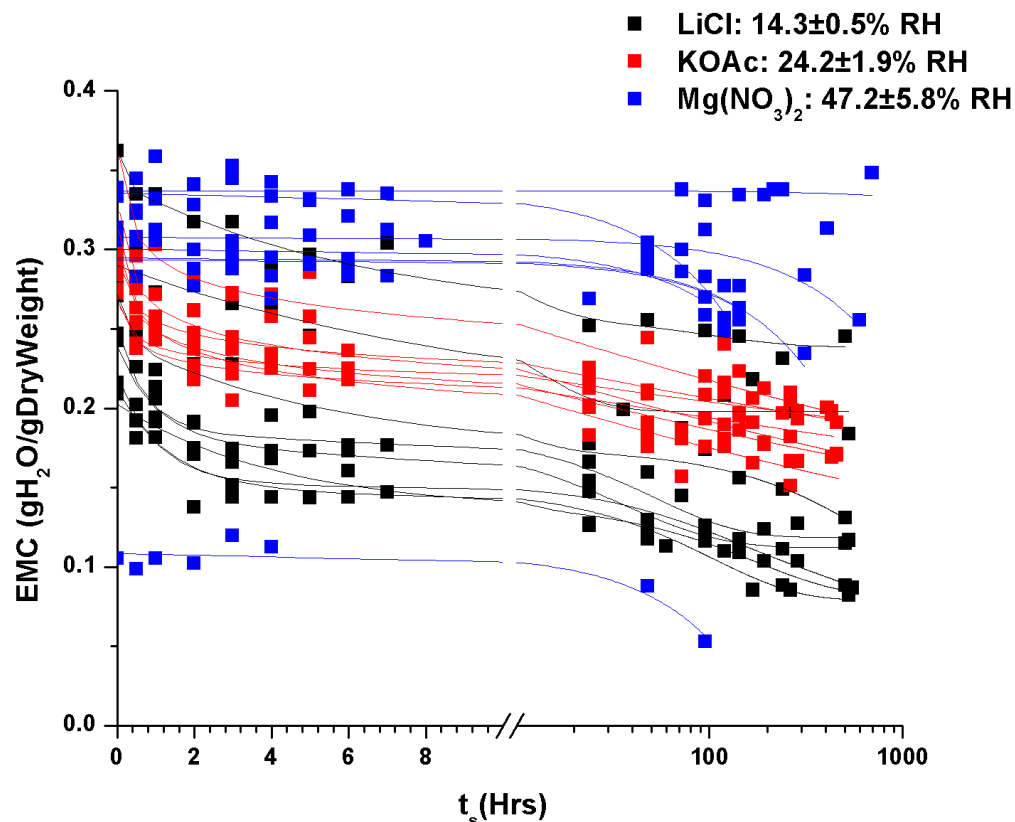
Figure 16: EMC as a function of storage time for all sets of RH.

3.3.2 PLI & Effect of Storage RH on Crystallization

PLI images were imported and analyzed in Matlab (R2017B). Each polarized image (image taken with crossed polarizers) was changed to a grayscale intensity image. A threshold intensity was established by finding the average maximum value of intensity of an area outside the sample plus two standard deviations. All pixels with intensities below the threshold value were zeroed. This was done to remove noise from the camera and particulates which could affect the polarization state of light. Crystal area was then measured by the number of pixels with intensity higher than zero in the crossed polarizer image of a user defined area from the uncrossed polarizer image. It is important to note

that measured crystal area included noise from dust and particulates that also polarized light however this signal was present in all successive images and did not factor into measurement of crystal growth. For each set of RH crystallization as a function of storage time was graphed. Figure 17 is an examples of the images obtained. Panel a) shows the white light image of the sample and b) the corresponding crossed polarizer image after Matlab processing. The white area is crystallization present in the sample.
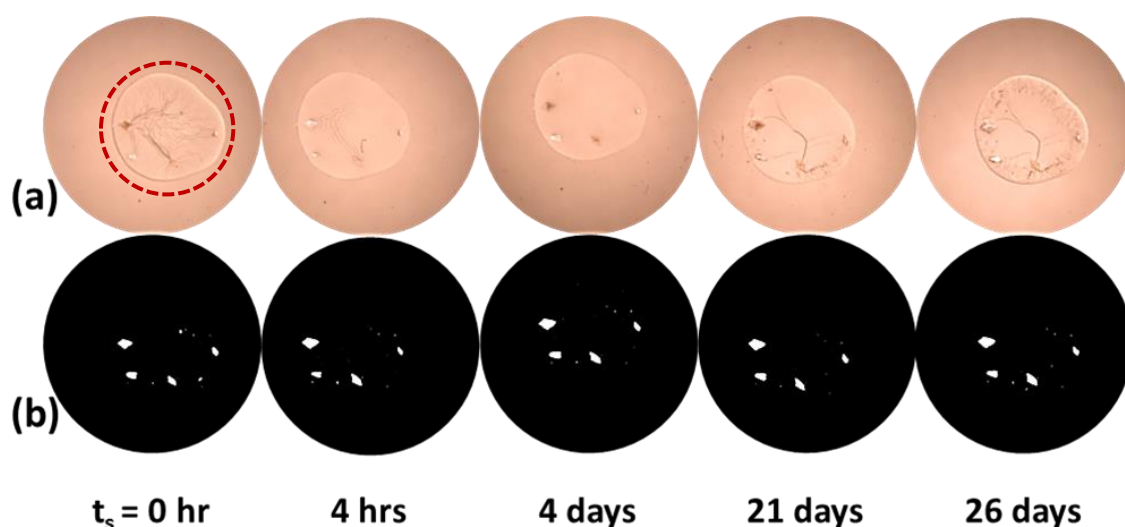
Figure 17: Time progression of samples stored in LiCl saturated salt low RH containers. The red circle indicates the sample, the surrounding area is the coverslip. a) Samples imaged through uncrossed polarizers and b) samples imaged with cross polarizers and processed in Matlab for crystal area measurement.

Figure 17 shows the progression of a characteristic sample during storage at 14.3±0.5% RH. At this RH there were three distinct phases that occurred during storage: crystallization, wrinkling, and desiccation cracking. Crystallization occurs as water evaporates from a sugar solution. As the water evaporates the solution saturates and

forms a precipitate in the form of a sugar crystal.[48] In order for this to happen the evaporation has to be slow enough that the sugar has time to align itself into its crystalline pattern. The goal of LAD is to speed up evaporation enough so that this does not occur; however, some crystallization may result during processing or form over time as the amorphous solid relaxes. Samples immediately post processing had a 62.5% chance of having a small initial crystal. There was no relationship between initial crystallization and EMC post processing.

Figure 18 shows the crystal growth as a function of storage time for LAD processed and air dried samples. We see that air drying resulted in the highest amount of crystallization during storage with an exponential increase of crystallized area within 10 hours of storage corresponding to the time for which they experienced an exponential decrease in moisture content. They reached a moisture loss limit after 10 hours corresponding to the time at which crystal growth stopped.
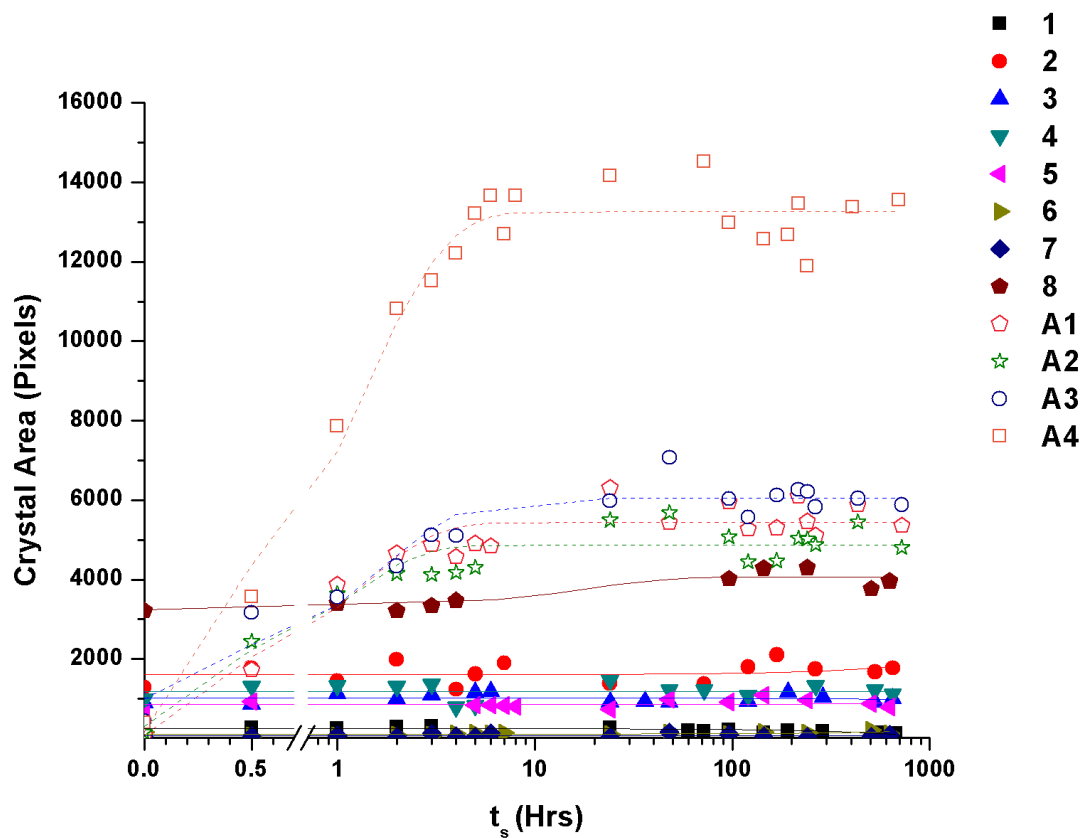
Figure 18: Crystal area as a function of storage time for air dried (A1-A4: exponential fit) and LAD (1-7: linear fit, 8: exponential fit) processed samples stored at 14.3±0.5% RH.

Of the 8 LAD processed samples (Figure 19) three had initial crystal area less than 500 pixels, upon inspection of their crossed and uncrossed polarizer images we concluded that those three samples (1,6,7) did not have initial crystals and that the measured pixel area was equivalent to the dust measured in a sample free region.
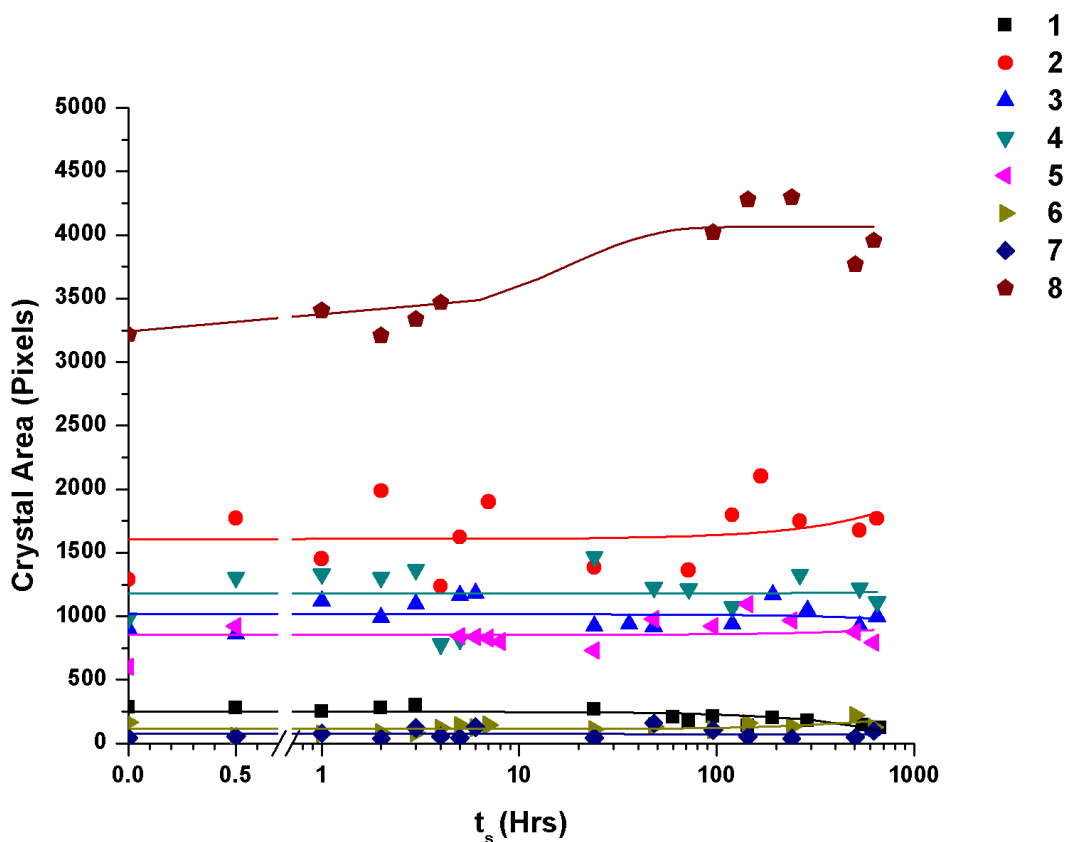
Figure 19: Crystal area as a function of storage time for LAD processed samples stored at 14.3±0.5% RH.

The LAD samples with initial crystal area between 500 and 2000 pixels experienced minimal linear crystal growth during storage corresponding to their slight linear decrease in EMC. One LAD sample (8) contained an uncharacteristically large amount of crystallization (>3000 pixels) post LAD followed by an exponential increase

in crystal area. Sample 8's uncharacteristically large initial crystal could have been caused by a larger particulate in the sample acting as a crystal seed. After approximately 100 hours of storage samples experienced a halt in crystal growth corresponding to their moisture loss limit.

This was also the earliest onset time when desiccation cracking was observed. Cracking was observed beginning on the edge of the drop. This exterior to interior crack formation indicates that a gel ring was forming on the edge and moving inward as the sample evaporated. The gel/ substrate interface allowed for adhesion while the gel/ air interface allowed for evaporation, when these processes competed tensile stresses caused cracks to form.[49] This is in agreement with studies done on cracking of sessile droplets by other groups. They have observed the same exterior to interior radial cracking and found that cracking depends on the concentration gradient within the sample. This gradient is dependent on drying rate.[50,51] The average storage time for desiccation cracking to begin was t_s=324±159 hours.

Wrinkling of the samples, as shown in Figure 17 (a) at t_s = 0 hr, only occurred when they were removed from their low RH environments into the higher RH of the room. It also only occurred during the first few hours after processing (t_s= 4±1.7 hrs). When placed back in low RH wrinkling dissipated quickly. Alternatively, if left for a longer period of time in high RH the sample eventually reached equilibrium and the wrinkling disappeared. This likely resulted from a change in volume at the surface of the sample.[52] The samples mass distribution reached equilibrium while being processed at a low RH. When placed in a higher RH the surface absorbed moisture from the air causing

it to superficially swell. The interior of the sample, which was contact pinned to the substrate, was no longer in equilibrium with the surface resulting in wrinkling.

The second set of samples was stored at 24.2±1.9% RH. Figure 20 shows crystal area as a function of storage time for both LAD processed and air dried samples. Air dried samples experienced the largest crystal growth over time. They experienced exponential growth during the first 2 hours, corresponding to the exponential decrease in EMC, followed by a halt in growth. This excluded one air dried sample (A2) which did not form a crystal during storage at all; its measured initial crystal area was below 500 pixels and determined to be noise from particulates. Out of the LAD processed samples six (2-7) contained a small amount of initial crystallization, of which five (2,3,5-7) experienced a slight exponential crystal growth in the first 10 hours, corresponding to the largest drop in EMC, followed by no growth. The sample (4) with an initial crystal area below 1000 pixels only experienced a slight linear increase in growth. None of the samples stored at this relative humidity underwent wrinkling or cracking.
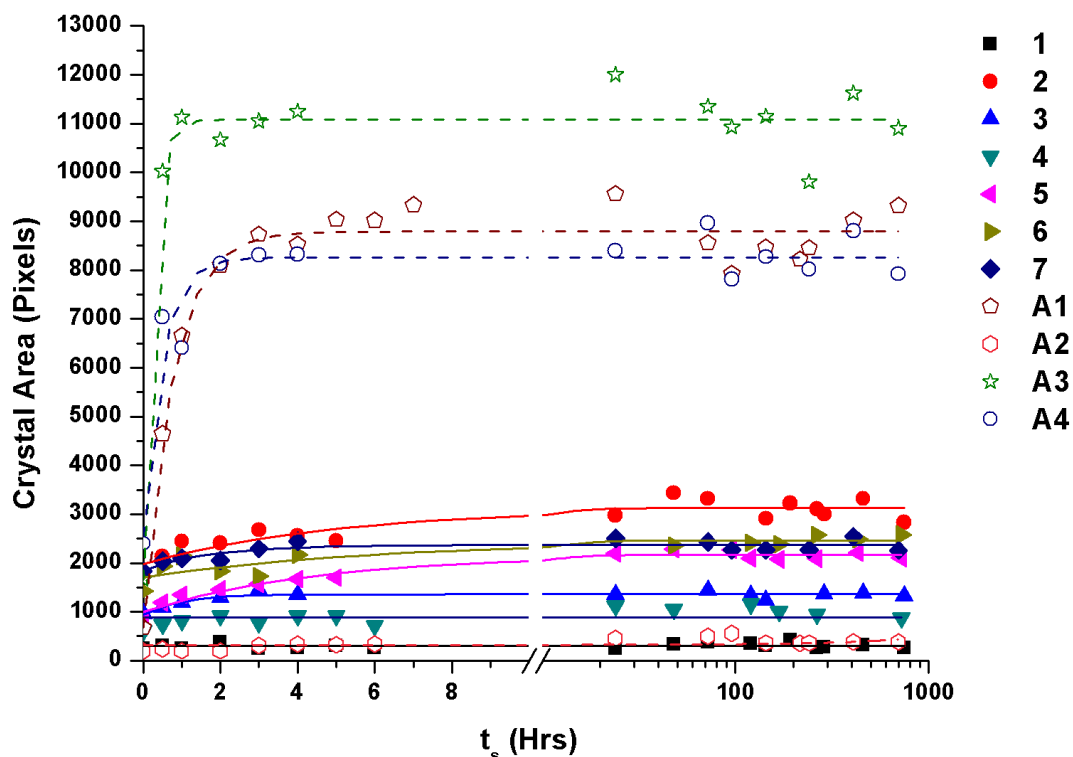
Figure 20: Crystal area as a function of storage time for air dried (A1, A3, A4: exponential fit, A2: linear fit) and LAD (1,4: linear fit, 2,3,5-7: exponential fit) processed samples stored at 24.2±1.9% RH.

The final set of samples were stored at 47.2±5.8% RH, Figure 21 shows the crystallization area as a function of storage time for LAD processed and air dried samples. Both air dried and LAD samples, with the exception of sample 3, crystal area increased non-linearly over storage time before reaching maximum crystallization. Air dried samples reached maximum crystallization faster than LAD processed. Air dried samples highest rate of crystallization and highest rate of evaporation both occurred within 2 hours of storage. LAD samples highest rate of crystallization occurred after 10 hours of storage which corresponded to the start of a linear decrease in EMC. Sample 3

had initial crystals upon removal from LAD but did not experience any crystal growth over time corresponding to its constant EMC over storage. This agrees with the trend that evaporation rate determines crystallization rate.
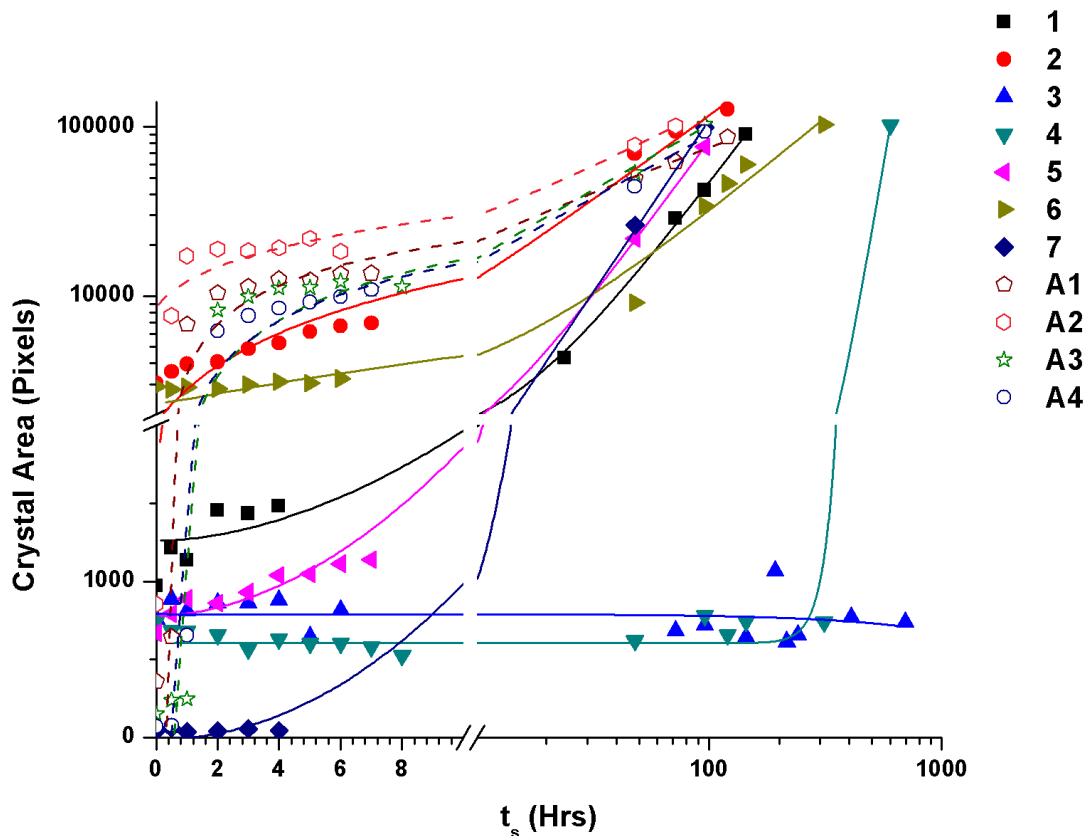
Figure 21: Crystal area as a function of storage time for air dried (A1-A4: power fit) and LAD (1, 2, 4-7: power fit, 3: linear fit) processed samples stored at 47.2±5.8% RH.

3.3.3 SWLI

SWLI was used to characterize the topography and thickness of LAD processed samples. Figure 22 shows a color map of sample height. Two cross sections are marked by red and black dashed lines and their corresponding profiles are displayed. The slope of the edges of the samples was outside the range of measurement capable by the Nexview,

these areas display as zero height. The coverslip height shown on the edges of the profile was used as the base of the sample and subtracted from sample height to obtain thickness.
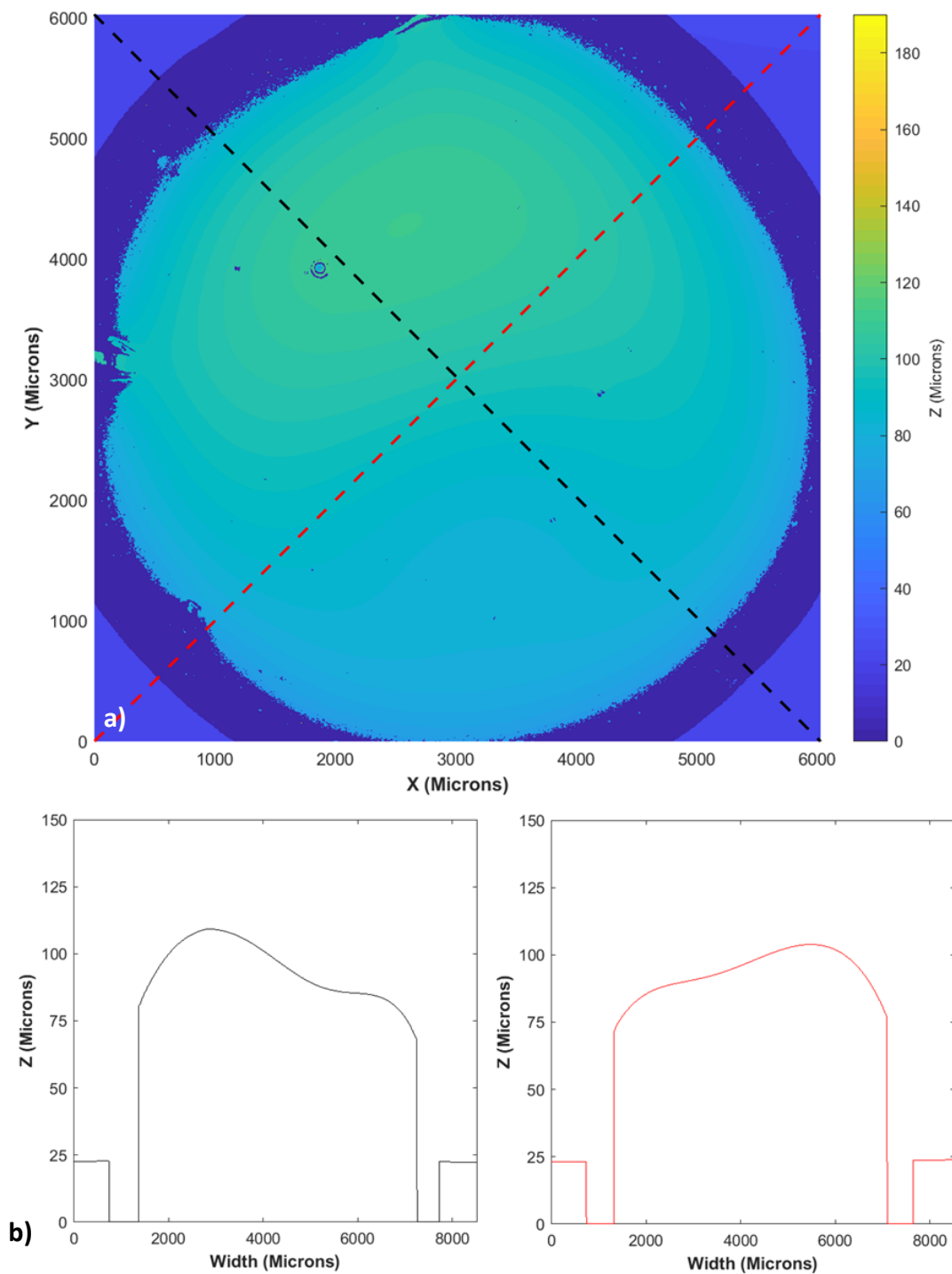
Figure 22: a) Color map of the height across sample, blue and red dashed lines are b) associated cross sections height profiles.

The average maximum thickness of LAD processed samples one day after storage (~14% RH) was 90.81 ±6.53 microns with an EMC of 0.16±0.04 gH_2O/gDryWeight. The average decrease in maximum sample thickness after 27 days of storage (~14% RH) was 8.65±1.71 microns corresponding to a decrease in EMC of 0.04±0.02 gH_2O/gDryWeight. There was no statistically significant relationship between a decrease in EMC and a decrease in sample height, most likely because the changes were on such a small scale.

Profiles taken from all samples indicate that there is variability in thickness across the sample. A majority of samples exhibited a dome shape profile with the thickest part of the sample lying slightly off center. A few samples also showed a slight off center dip in the profile as well. The shape of the profile did not change over storage just the overall thickness. The off center nature could potentially be from variability of the position of the laser within the sample during processing.

SWLI was also used to determine whether cracking after storage at 14.3±0.5 % RH was occurring on the sample/coverslip or sample/air interface. Figure 23 shows a comparison of a cracked samples SWLI color map, non-interferometric image, and corresponding profiles. We see in the non-interferometric image that the cracks extend all the way across the sample; however, they do not show up on the height profile. This implies the cracks must be subsurface on the sample/ coverslip interface. This is supported by the fact that we can see white light interference fringes in Figure 23 (a) from the thin air gap that is forming from delamination. Delamination could potentially comprise sample integrity.
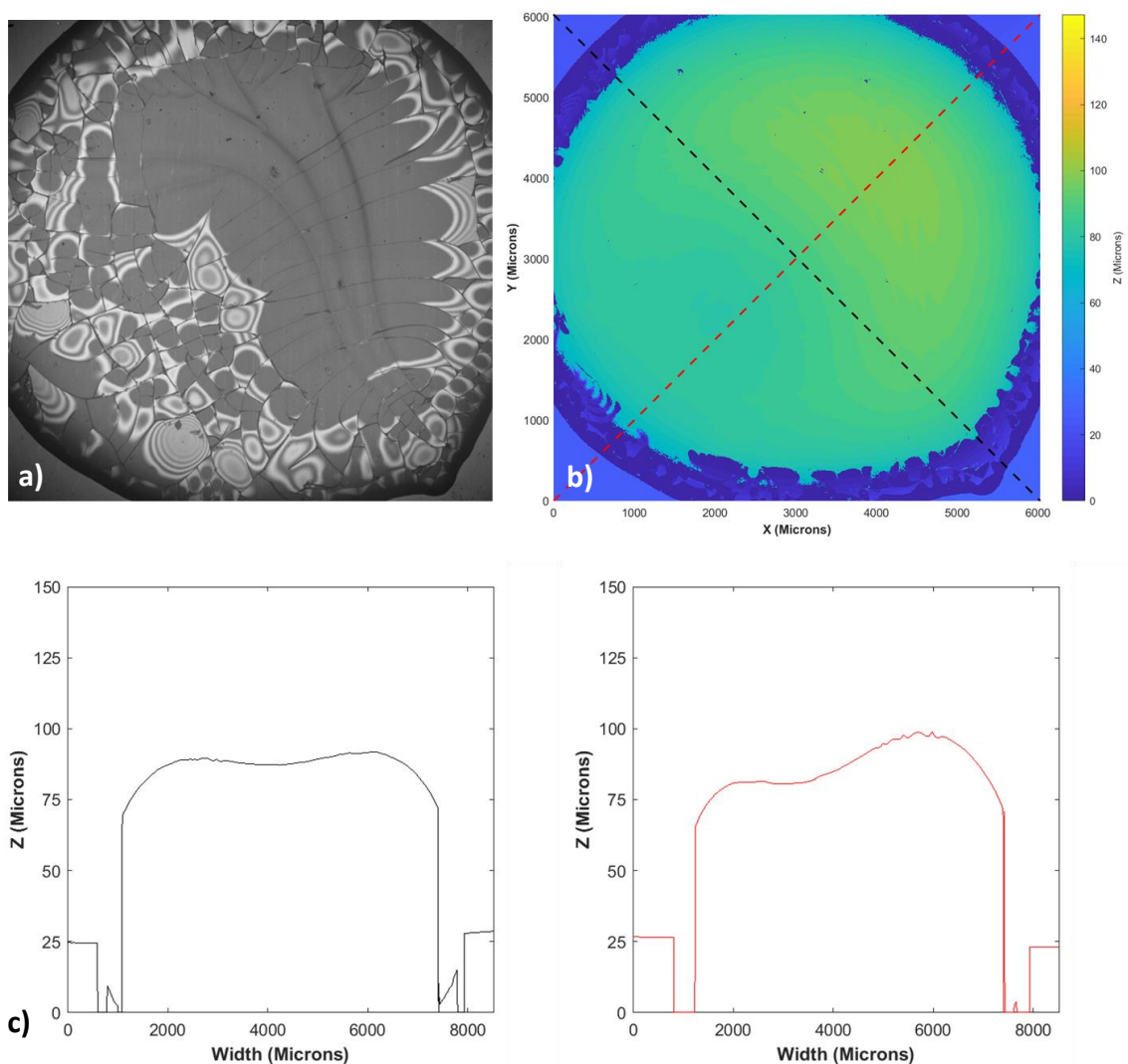
Figure 23: LAD processed sample after 27 days of storage at 14.3±0.5% RH. a) The non-interferometric image and b) the SWLI height map with corresponding c) height profiles.

3.3.4 Raman Spectroscopy

Figure 24 shows the difference in Raman spectra of crystalline trehalose and amorphous trehalose. Crystalline trehalose has very well defined, narrow bands while the amorphous bands are broadened. Because crystals possess long-range translational symmetry they have quantized lattice vibrations, and this limits the number of Raman

active vibrational modes. The amorphous form does not have spatial order so vibrational modes are not limited by lattice vibrations. This means that all the vibrational modes are sampled resulting in band broadening.[53]
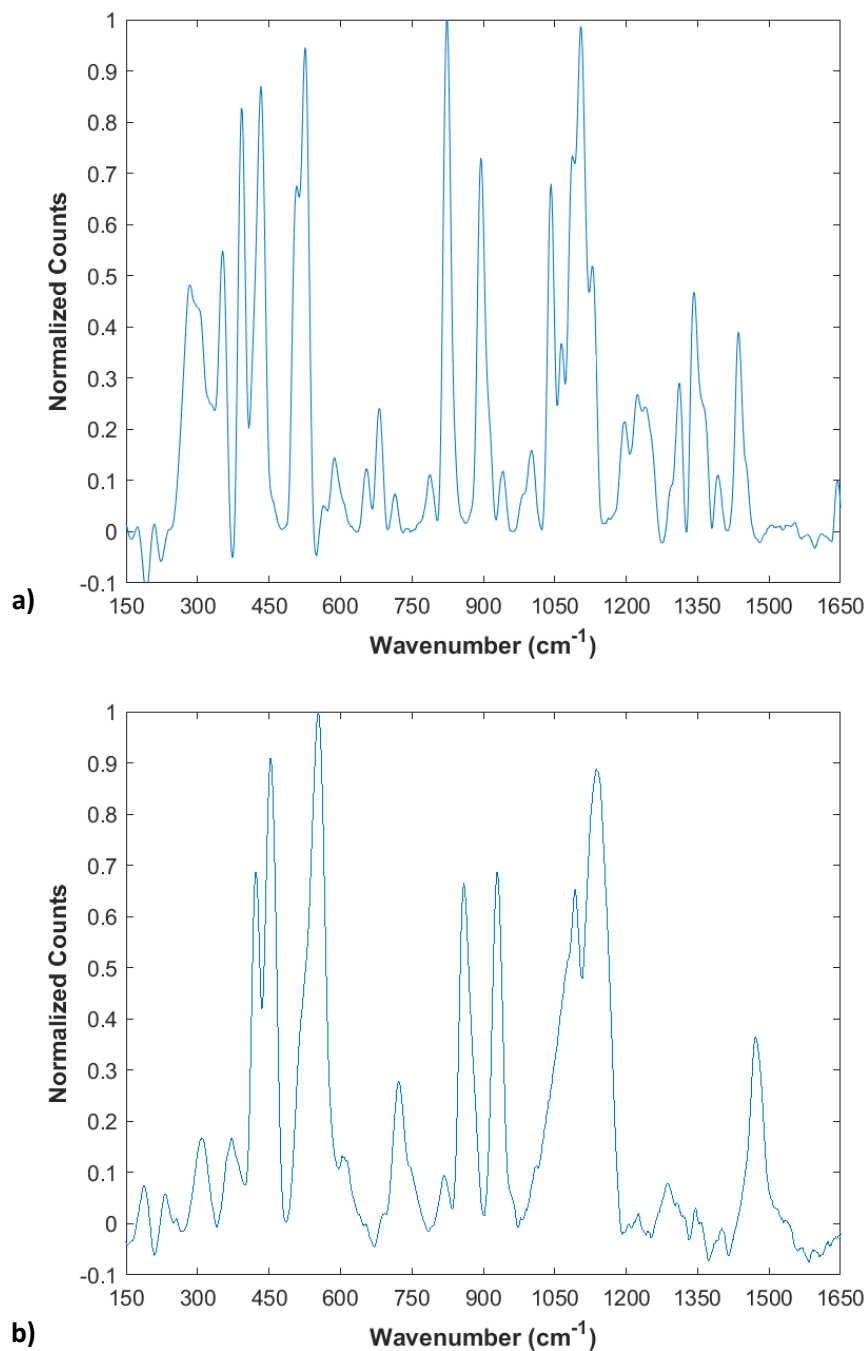
Figure 24: Raman shift spectra of a) crystalline trehalose and b) amorphous trehalose.

Spectra were acquired at three transverse locations across a LAD sample to measure the relative distribution of trehalose across the sample. This was coupled with SWLI of the same sample to determine the relationship between thickness and trehalose distribution. Figure 25 is a SWLI cross section of a sample with the Raman spectra locations marked and the corresponding spectra at each location. First we note that the Raman spectrum for trehalose is present at each location indicating that the sugar is distributed across the sample. Comparing each sample set of spectra to the corresponding thickness measurement yielded no relationship. We do see that the trehalose at each location is in the amorphous state and not crystalline.
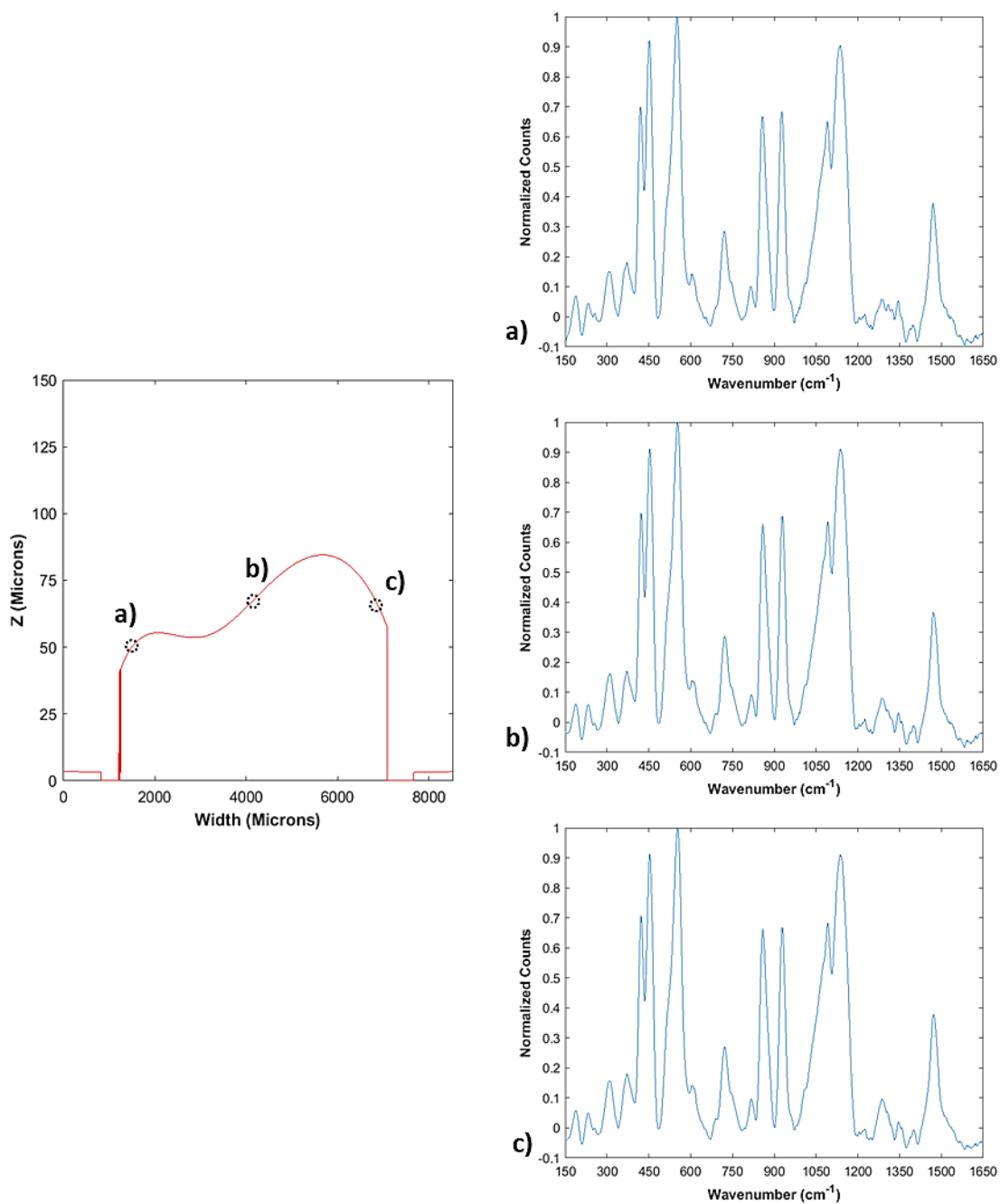
Figure 25: A SWLI height profile on the left is marked with three locations that correspond to the normalized Raman spectra on the right.

3.4   Discussion

PLI of LAD processed samples stored for an extended time at low RH shows promise for the long term stability of samples. Out of the three storage RH the lowest (14.3±0.5% RH) is the most logical option. Compared to the other two RH, crystallization for LAD processed samples was negligible. This reduces the risk of degradation during storage of proteins that are sensitive to the mechanical stresses of crystallization. However, initial crystallization of the sample during LAD processing indicates that the samples need to be dried faster to overcome crystallization during processing. Samples with very large initial crystal area have a higher likelihood of substantial crystal growth during storage. This will require a higher power LAD source or an alternate wavelength with a higher absorption coefficient in water. Both of these options would accelerate the drying time of LAD and potentially reduce initial crystallization that could act as a seed crystal during even longer storage times. These studies also revealed a phenomenon that we had not accounted for, desiccation cracking. Cracking during storage is unfavorable and could damage the embedded proteins and reduce storage life. Potential solutions include pushing the samples to an even drier state during LAD processing by changing the source, as mentioned previously, or lowering processing RH. Alternatively we could raise the storage RH high enough to lower evaporation to prevent competition with the gel/substrate adhesion but keep it low enough to maintain an amorphous state.

SWLI showed that cracking was subsurface and accompanied by delamination of the sample. A potential solution for this could be a substrate change to something more flexible to contract and expand as the sample reaches very low EMC. Raman

spectroscopy indicated that trehalose was in an amorphous form throughout LAD samples. While SWLI coupled with Raman spectroscopy did not yield a relationship between relative trehalose concentration and sample thickness, it did show that trehalose was distributed across the sample. The lack of correlation could mean that trehalose is evenly distributed across the sample regardless of thickness.

CHAPTER 4: PROTEIN FUNCTIONALITY STUDIES

4.1   Introduction

The field of biologics has seen rapid growth in the past few decades because of an exponential increase in diagnostic and therapeutic target discoveries.[2] Protein based biologics are used in therapeutics and diagnostics and have been developed to treat diseases ranging from arthritis and psoriasis to cancer.[54] A challenge in the development of protein-based diagnostics and drugs is maintaining the protein in the folded state during processing and storage as the three-dimensional structure of the protein is often responsible for its functional activity.[5–7] Long-shelf lives for proteins have been achieved by freeze drying, also known as lyophilization, however the complexity, processing time, high cost and potential for instability during processing and storage are disadvantages of this technique.[13,55,56] Even after lyophilization most proteins still have to be stored below 4°C.[11] Recent research has demonstrated that anhydrous, or dry state, preservation in a trehalose amorphous (non-crystalline) solid matrix may be an alternative to freeze drying for the preservation of biological samples.[9–10] We have previously described a new processing technique, light assisted drying (LAD), to create trehalose amorphous solids for the preservation of biologics. LAD uses illumination by near-infrared laser light to assist in the formation of trehalose amorphous solids. Static air-drying of sugar solutions is dominated by evaporative cooling which causes the drying rate to slow substantially

and allows for crystallization of the sugars. LAD selectively heats water to overcome cooling due to evaporation and speeds dehydration of the samples. As water is removed from the sample, the remaining sugars and salts become concentrated, and, as long as the solutes do not crystallize, the viscosity increases with progressive water loss until an amorphous solid is achieved. Samples need to be stored below the glass transition temperature, T_g, of the trehalose matrix to prevent degradation.[27] Our previous work has demonstrated the effectiveness of LAD to reach end moisture contents (EMCs) low enough for storage at elevated temperatures in the glassy state and determined the optimal LAD processing parameters for achieving these EMCs.[57] We have also characterized sample morphology and distribution of the glass forming matrix, as well as, the subsequent storage conditions for optimal sample stability.[58] This chapter addresses the functionality of proteins embedded in LAD processed samples. It also discusses the effect of protein concentration and size on EMC to determine whether LAD is universally applicable or would need to be optimized for each protein of interest. First, we measured the EMC at a specific LAD processing time of different protein concentrations and three different protein sizes. We then tested functionality of a model protein, lysozyme, immediately after LAD processing and after extended storage using a standard activity assay.

4.2   Methods

The LAD system with the 1064 nm laser and 1850 nm laser (as described in Chapter 1) was used for processing. Samples consisted of 40µl droplets containing a model protein in a drying solution (DS). Proteins were mixed into the DS and the dry weight was adjusted using the protein concentration to include the mass of the protein.

For each test, a 40 μL droplet of the protein in DS was deposited onto an 18mm diameter borosilicate glass coverslip (12-546, Fisherbrand) substrate and the initial mass was determined gravimetrically using a 0.01mg readability balance (AS 82/220.R2, RADWAG). The sample was then moved into the humidity chamber for laser irradiation. The temperature of the sample was monitored during processing using the thermal camera. After irradiation, the sample was removed from the humidity chamber and immediately massed again to determine EMC.

4.2.1   Protein Concentration & Size

Samples (N=3 for each study) were LAD processed with the 1850 nm laser for 10 minutes at a power density of 4.04 W/cm^2 corresponding to a maximum sample temperature of T_{max} =72.9±2.0°C. For the protein size study, we used egg white lysozyme (LS002933, Worthington Biochemical), ß-galactosidase (LS004090, Worthington Biochemical), and peroxidase (LS002559, Worthington Biochemical). Concentration of lysozyme, ß-galactosidase, and peroxidase was verified using the absorption of light at 280 nm, 275 nm, and 280 nm, respectively, with a microplate spectrophotometer (Bio-Tek Synergy HT). Size was defined as proteins hydrodynamic radius, the radius of an equivalent hard sphere diffusing at the same rate as the protein, (see Table 4) and each protein was used at a concentration of 0.5 mg/ml. The protein concentration study used lysozyme at 0.5, 10, and 25 mg/ml for testing. Sample EMC was determined immediately after processing.

Table 4: Proteins used in the protein size study and their corresponding hydrodynamic radii taken from various sources.[59]–[61]

Protein	Hydrodynamic Radius (nm)
Lysozyme	1.9
Peroxidase	3.0
ß-galactosidase	6.9

4.2.2 Lysozyme Functionality

All samples for the functionality studies consisted of 0.5 mg/ml lysozyme in DS. The functionality of lysozyme in each sample was measured using the assay described by Worthington Biochemical for the rate of lysis of Micrococcus lysodeikticus cells.[62] The assay was altered to fit a 96-well format and measured the decrease in turbidity as a function of time at 450 nm, $\Delta A450/min$, referred to as the response rate. We calculated the specific activity of each sample using the measured concentration and $\Delta A450/min$.

The first functionality study used LAD with the 1064 nm laser at a maximum sample temperature, T_{max}, of 43.0±1.8°C. All LAD – 1064 nm processed samples (N=5) were heated with the 1064 nm laser for 60 minutes at a power density of 26.9 W/cm^2. Air drying of samples (N=3) for 60 minutes at 11% RH was used as a comparison. Samples were assayed at three different times $t_s = 0$, 1, and 27 days after LAD processing/ air drying. After LAD processing samples were stored individually in small volume containers above a saturated salt solution of lithium chloride (LiCl) (ChemCenter) at 14.3±0.5 % RH. This was measured with an RH probe (HH314A, Omega). We chose

these storage times and the storage RH based on the results from our previous optical characterization work. The t_s = 0 days determined the functionality of embedded lysozyme immediately after LAD, t_s = 1 day allowed the samples to reach a lower EMC and lower their evaporation rate to a negligible value, and t_s = 27 days allowed subsurface cracking to occur so we could investigate its effects on embedded proteins. The three air dried samples were stored at a higher RH of 47.2±5.8% to promote crystallization of the sample and to assess the impact of crystallization on protein functionality.

A 0.5 ml aliquot of the stock solution was kept at ambient temperature for 27 days and also assayed for comparison. In addition, a 0.48 ml volume of the sample was also incubated in a water bath at ~45°C for 60 minutes to compare the effect of heating without drying to LAD processed samples. Four 40µl droplets were taken from this sample, diluted with deionized water to a concentration of 0.1 mg/ml of lysozyme for use in the functionality assay. It should be noted that the temperature of the LAD samples decreased during processing due to evaporative cooling, while the water bath samples were held at a near constant temperature.

The second functionality study used LAD with the 1850 nm laser at T_{max} = 87.0±2.3°C. One LAD – 1850 nm sample was processed at 7.39 W/cm^2 for 6 minutes and assayed immediately after. A 500µL volume of the control solution was incubated in a water bath at ~90°C for 4 minutes as a comparison. Before assaying, samples were re-hydrated and then diluted with deionized water to a concentration of 0.1 mg/ml of lysozyme to achieve a linear response rate for the assay. The concentration of lysozyme for each sample was verified by measuring the absorption at 280 nm.

4.3   Results & Analysis

4.3.1   Protein Concentration & Size

Figure 26 shows EMC as a function of protein concentration. Note that all concentrations were processed under the same conditions (LAD with 1850 nm at $T_{max\ =}$ 72.9±2.0°C for 10 minutes. We do not see a change in average EMC based on protein concentration and each one is within each other's standard deviation. However, there is a decrease in standard deviation with increasing protein concentration. This could be because an increase in protein concentration means lower initial moisture content leading to less variability at lower EMCs. This is supported by results from Chapter 2 were we observed a decrease in EMC standard deviation at progressively lower EMC.
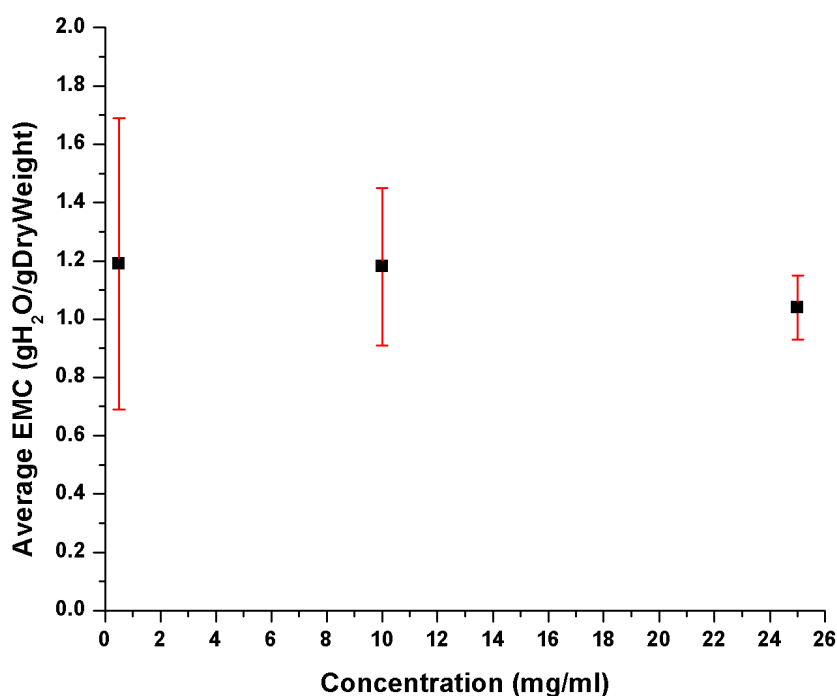
Figure 26: EMC v. protein concentration for lysozyme in DS, LAD processed for 10 minutes with the 1850 nm laser at a $T_{max} = 72.9\pm2.0$°C.

Figure 27 shows EMC as a function of protein hydrodynamic radius. Hydrodynamic radius is the apparent size of the solvated protein. Note that each protein is at the same concentration (0.5 mg/ml) and processed under the same conditions as listed for the protein concentration test. Lysozyme, peroxidase, and ß-galactosidase are 1.9, 3, and 6.9 nm respectively. We do not see a change in EMC with increasing hydrodynamic radius. However, we see the same decrease in standard deviation with increasing protein size that we observed with increasing protein concentration. This could be attributed to the same lower initial moisture content theory as described previously.
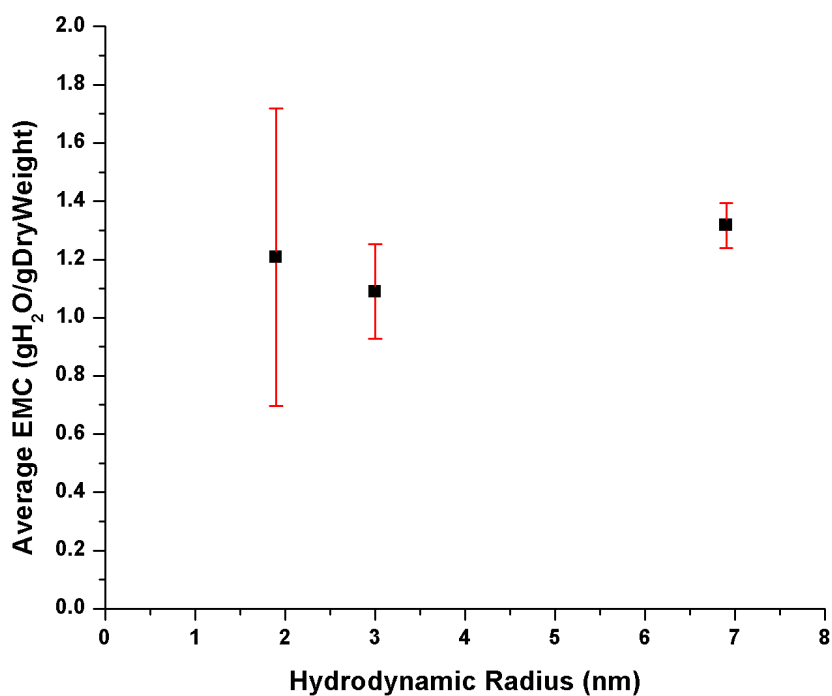
Figure 27: EMC v. hydrodynamic radius of proteins in DS, LAD processed for 10 minutes with the 1850 nm laser at a $T_{max} = 72.9\pm2.0°C$.

The average EMC for each study indicate that protein concentration and size might not affect the EMC of LAD processed samples under the same processing parameters; however, the decrease in standard deviation with increasing protein concentration and protein size needs further investigation. The decrease could be caused by lower initial water content in which case LAD processing parameters might have to be adjusted on an individual protein-by-protein basis, or it could be an artifact of a low sample number and increasing N might show the same standard deviation regardless of protein concentration and size. This would imply that one set of processing parameters could be universally applied to most proteins. A larger sample size needs to be performed and a more exhaustive range of protein sizes and concentrations needs to be tested to determine the limits of this study.

4.3.2   Lysozyme Functionality

This study addressed the functionality of proteins processed with LAD. Figure 28 shows the standard activity for each set of samples assayed as described in the methods section. Standard activity for a lysozyme assay is a measure of how well lysozyme destroys micrococcus lysodeikticus cells; as functional lysozyme destroys cells the turbidity of the water decreases over time and the absorbance of 450 nm light decreases. Therefore the rate at which absorbance at 450 nm changes over time depends on the functionality of lysozyme as well as the concentration. A higher percentage of denatured lysozyme will result in a lower rate of change of A_{450}. Standard activity (SA) is measured as

$$SA = \frac{(\frac{\Delta A_{450}}{min}*1000)}{m_{lys}} \qquad \text{[Equation 6]}$$

where $\frac{\Delta A_{450}}{min}$ is the rate of change of absorbance over time, 1000 is a conversion factor to

units, and m_{lys} is the mass of lysozyme in the reaction.
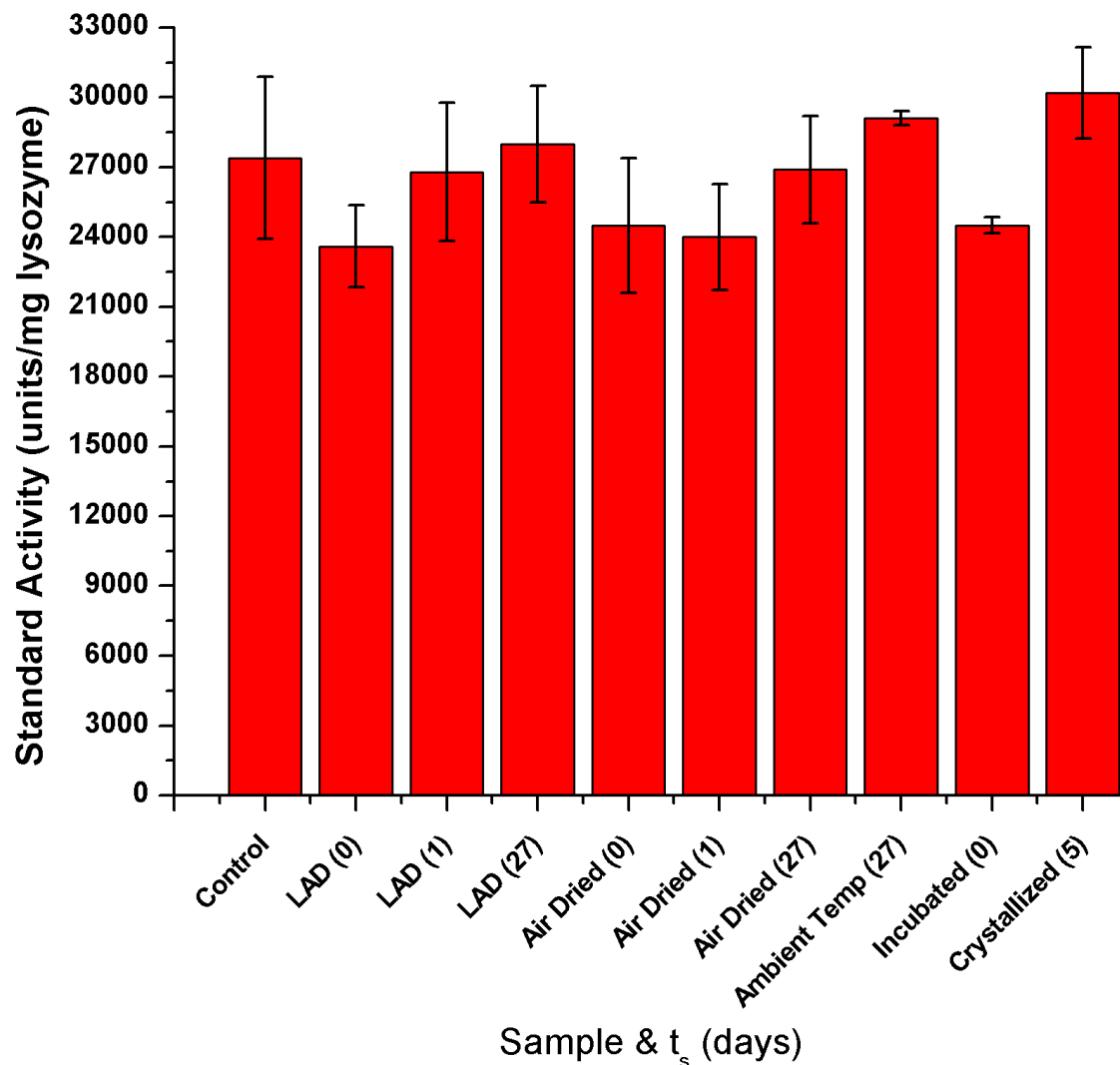
Figure 28: Standard activity of lysozyme for unprocessed refrigerated control solution, LAD processed, air dried, incubated in a sealed container (~45°C), ambient temperature storage, and crystallized samples. The numbers in parenthesis next to each sample label is the storage time in days before assaying.

We see no significant change in functionality compared to the control solution for either LAD or air dried samples. All variations in the average functionality of test

samples fall within the standard deviation of the control. This implies that LAD does not have a negative effect on protein functionality during processing or subsequent initial storage. Because the incubated sample functionality was also unaffected we can assume that thermal denaturation did not occur. The average EMC of LAD samples at $t_s = 0$ days and $t_s = 1$ day was 0.12 ± 0.02 and 0.06 ± 0.01 gH$_2$O/gDryWeight respectively. Extremely low EMC did not have an effect on protein functionality. Air drying, ambient temperature storage, and crystallization also did not show a loss in functionality. Lysozyme is a robust protein.

Figure 29 is standard activity of the preliminary functionality study of LAD at elevated temperatures utilizing the 1850 nm laser. We see that the control solution that was kept at 8°C has the highest SA. The LAD processed sample shows a small decrease in functionality compared to the control. The incubated sample has the lowest functionality, this is indication that the protein underwent thermal denaturation. Not only was the LAD sample processed for the same amount of time as the incubated sample at a comparable temperature (~90°C) but it was also processed for 2 minutes longer at a slightly lower but still potentially damaging temperature (76.9±10°C). This indicates that LAD processing has the potential to use elevated temperatures to speed up the drying process without damaging the embedded protein.
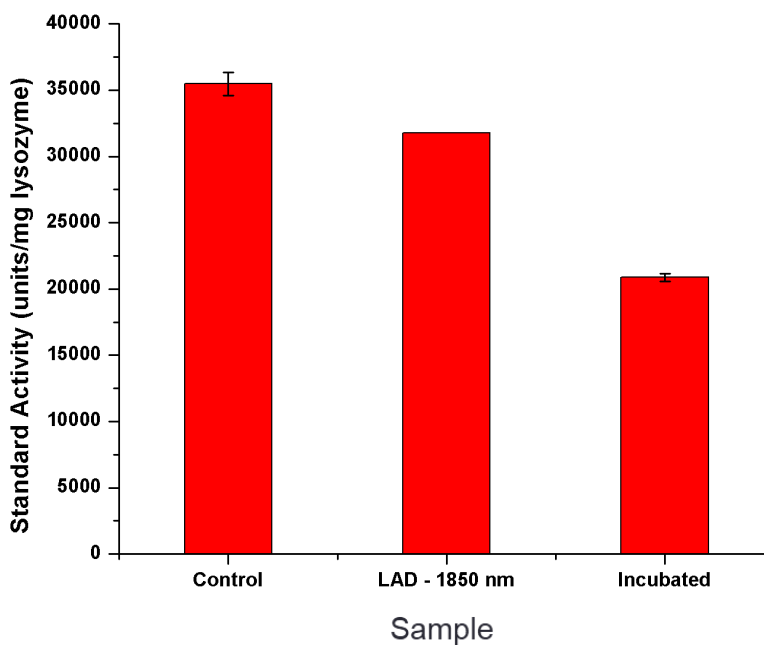
Figure 29: Standard activity of lysozyme in DS samples for unprocessed refrigerated control solution, LAD processed with 1850 nm. and incubated at a comparable temperature (~90°C). The LAD - 1850 nm sample has no standard deviation, only one sample was processed and tested.

Proteins processed via LAD at elevated temperatures do not appear to be thermally denatured as would be expected. This is most likely because of the thermal gradient across the sample. Looking at Figure 30 we see thermal images of the LAD – 1850 nm sample. Figure 30 (c) shows the thermal profile across the droplet at the processing time corresponding to maximum sample temperature. We see that the entire droplet is not at 90°C. The temperature profile is Gaussian and decreases down to <40°C on the edges. Marangoni flows develop within sessile drying droplets because of the thermal gradient across them associated with evaporative cooling. LAD increases that thermal gradient and we believe that it further increases the rate of recirculation within the droplet. This recirculation might mean that proteins are being pushed towards the edge of the droplet

into cooler areas and then back along the surface towards the center where they are exposed to higher temperatures. This potential protein circulation across the drop would allow them to dry without experiencing constant elevated temperatures that would denature them.

Figure 30: Thermal image of sample a) before LAD processing, b) during LAD processing at maximum temperature, and c) the corresponding thermal profile across the sample taken from b). The dashed black circles in a) and b) indicate the location of the sample.

4.4   Discussion

Varying protein size and concentration did not affect the average EMC of samples when processed with the same LAD parameters,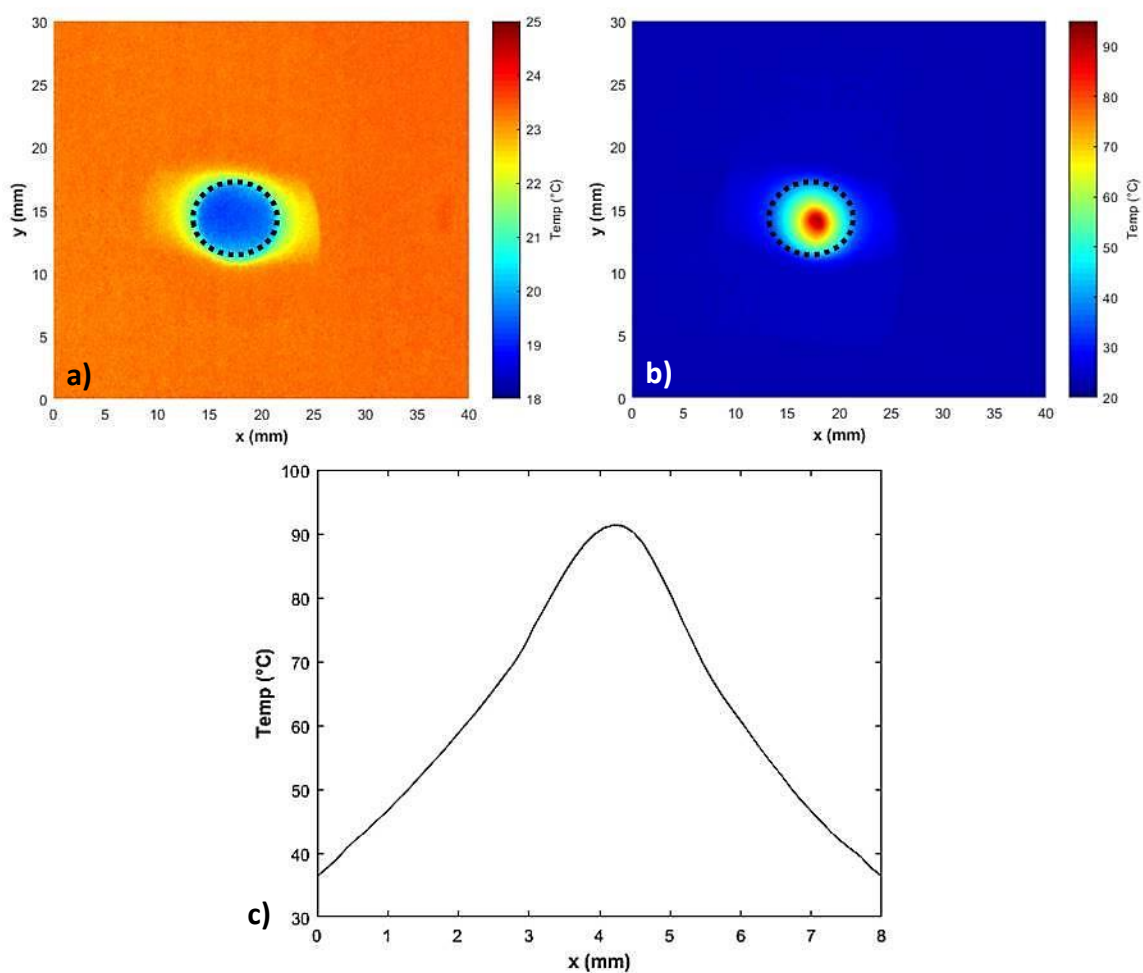 but the standard deviation decreased with increasing concentration and size. Increasing the sample size (N) of this study will help determine if the standard deviation variability is truly related to concentration and size. The average EMC of all the samples indicates that LAD could potentially be applicable to a wide variety of proteins using one processing parameter set. This is beneficial for use on an industrial scale, many pharmaceutical companies produce products with a wide variety of proteins and having a universally applicable processing parameters means that LAD would not have to be optimized for individual proteins. However, this study will need to be expanded to test the limits of LAD in regards to a universal parameter set as there is likely a maximum concentration at which EMC will start to vary.

The lysozyme functionality study indicates that LAD processing with the 1064 nm laser at $T_{max} = 43.0 \pm 1.8°C$ does not affect the functionality of lysozyme. This data coupled with the water bath incubated samples implies that thermal denaturation is not occurring which makes sense because the processing temperature is well below the approximate unfolding temperature of lysozyme (~70-80°C depending on solution).[63] LAD and air samples reached EMCs that were below 0.1 $gH_2O/gDryWeight$ (corresponds to a storage temperature above room temperature) without denaturing. This means that very low EMC does not affect functionality. These results are promising for the ability of LAD to produce samples without denaturing the embedded protein. The preliminary LAD – 1850 nm functionality study shows the ability of LAD to process

proteins at temperatures larger than the unfolding temperature without a substantial loss of functionality. Because this study was limited in scope it will need to be expanded to definitively prove that LAD can not only process samples at elevated temperatures without thermal denaturation, but also show the effects of EMC on sample functionality.

CHAPTER 5: CONCLUSIONS

The overall goal of this project was to develop a light based drying technique for the formation of amorphous trehalose to stabilize proteins for long term storage at elevated temperatures. The study was divided into three parts to test the performance of the system and the stability and structure of the resultant samples.

The first study tested the design of our LAD technique and its ability to reach low EMCs. We determined the effect of varying processing wavelength, power, and sample substrate on the EMC of samples dehydrated with LAD. Two wavelengths were used to assess the relationship between optical penetration depth in water and EMC. Two wavelengths with different absorption coefficients in water were compared by processing at powers that reached the same sample temperature. We found that sample temperature governed the drying rate and as to be expected a higher absorption coefficient in water yielded a higher temperature sample at a lower power. LAD was able to push samples to EMCs of interest for storage at potentially supra zero temperatures. We also found that filter paper produced the driest samples in the shortest amount of time. Moving forward the optimal LAD processing parameters would have been with the 1850 nm laser on filter paper; however, we did not have access to that laser for future studies. As a result we were not able to process samples on filter paper for future studies either because of the inability of the 1064 nm laser profile to be flattened without losing a substantial amount of power needed to reach processing temperatures of interest.

The second study optically characterized samples produced with LAD – 1064 nm at a maximum processing temperature of ~42°C on borosilicate glass coverslips. We used polarized light imaging to monitor crystallization kinetics of samples immediately post LAD processing and during storage at three different RH. We found that samples experienced minor crystallization during LAD processing and the optimal RH to inhibit crystallization over time was ~14% RH. During storage at this RH samples continued to evaporate to lower EMC. This implies a potentially higher storage temperature. However, cracking of the samples was discovered near the end of storage. We investigated this cracking with SWLI and determined that it occurred subsurface. We also used SWLI to show that thickness did not vary substantially across the sample; this has positive implications for solute distribution. Finally, Raman spectroscopy showed that there was an even distribution of amorphous trehalose across the sample. The results of the optical characterization study suggest that LAD processed samples stored at low RH are unlikely to crystallize over a long time scale. SWLI and Raman results imply that samples do have an even distribution of the preservation matrix in an amorphous which means proteins are more likely to be evenly distributed in their folded state.

Finally, we applied the findings of our previous work to the actual application of protein stabilization. We processed a model protein, lysozyme, with the LAD – 1064 nm system and tested their functionality with an activity assay. The 1064 nm laser had a limited maximum processing temperature well below the melt temperature of lysozyme. We found that being processed below that temperature with LAD did not denature the proteins; neither did reaching potentially damaging low EMCs. Compared to samples of the same solution that were heated in a water bath at a comparable LAD processing

temperature, stored in solution at 4°C and ambient temperature, and a final set that were allowed to crystallize there was no statistically significant change in lysozyme activity. This tells us that the LAD process does not have a unique negative effect on lysozyme functionality. A preliminary study was also conducted with the 1850 nm laser at a higher temperature ~90°C. This temperature is of greater interest because of its fast processing times but it could be potentially damaging to the protein. Comparing the functionality of LAD processed and water bath incubated lysozyme at temperatures above its melting temperature we found that LAD processed proteins maintained their functionality while incubated samples showed a substantial amount of partial denaturation. This suggests that elevated LAD processing temperatures could be used on proteins without thermally damaging them.

LAD is a more attractive option for anhydrous preservation of proteins compared to lyophilization and other preservation techniques because it is cost effective, fast, scalable, can be used for inline processing, can monitor sample temperature during processing, and has precise control over energy deposition. This dissertation has laid the groundwork for the LAD processing technique and shown its capabilities for stabilizing proteins at low EMC while still maintaining their functionality. Additional studies still need to be performed to further test the limits of LAD. This project would benefit from an alternate light source with a higher absorption coefficient in water to accelerate drying time. Also, this project only discussed the average EMC of samples. Future studies would benefit from knowing the spatial EMC to determine a more specific storage temperature range. Along the same lines, only overall average protein functionality was investigated because of the destructive nature of the lysozyme assay. The spatial distribution and

functionality of proteins needs to be determined to further optimize LAD processing. Green fluorescent protein is a viable option for a study of this nature because of its fluorescence dependence on functionality. Alternate proteins that are less robust also need to be tested to better understand the effect of LAD on proteins and if the processing temperature is universally applicable to most proteins or if it needs to be optimized on an individual basis.

REFERENCES

[1] Leader, B., Baca, Q.J., and Golan, D.E., "Protein therapeutics: a summary and pharmacological classification," Nature Reviews Drug Discovery 7(1), 21–39 (2008).

[2] Morrow, T., and Felcone, L.H., "Defining the difference: What Makes Biologics Unique.," Biotechnology healthcare 1(4), 24–9 (2004).

[3] Mease, P.J., Goffe, B.S., Metz, J., VanderStoep, A., Finck, B., and Burge, D.J., "Etanercept in the treatment of psoriatic arthritis and psoriasis: a randomised trial.," Lancet (London, England) 356(9227), 385–90 (2000).

[4] Angenendt, P., "Progress in protein and antibody microarray technology," Drug Discovery Today 10(7), 503–511 (2005).

[5] Hill, J.J., Shalaev, E.Y., and Zografi, G., "Thermodynamic and dynamic factors involved in the stability of native protein structure in amorphous solids in relation to levels of hydration.," Journal of pharmaceutical sciences 94(8), 1636–67 (2005).

[6] Stevens, and J, F., "A Novel Antibody Engineering Platform to Improve Antibody Stability," United States (2009).

[7] Ehrnsperger, M., Hergersberg, C., Wienhues, U., Nichtl, A., and Buchner, J., "Stabilization of proteins and peptides in diagnostic immunological assays by the molecular chaperone Hsp25.," Analytical biochemistry 259(2), 218–25 (1998).

[8] Zhu, H., and Snyder, M., "Protein chip technology," Current Opinion in Chemical Biology 7(1), 55–63 (2003).

[9] Wu, P., Castner, D.G., and Grainger, D.W., "Diagnostic devices as biomaterials: a review of nucleic acid and protein microarray surface performance issues.," Journal of biomaterials science. Polymer edition 19(6), 725–53 (2008).

[10] Wang, W., "Instability, stabilization, and formulation of liquid protein pharmaceuticals," International Journal of Pharmaceutics 185(2), 129–188 (1999).

[11] "Protein stability and storage," TR0043.1, Pierce Biotechnology, Inc., Rockford (2005).

[12] European Molecular Biology Laboratory, "Protein Purification - Storage of Purified Proteins," <https://www.embl.de/pepcore/pepcore_services/protein_purification/storage_purified_proteins/> (20 March 2018).

[13] Bjerketorp, J., Håkansson, S., Belkin, S., and Jansson, J.K., "Advances in preservation methods: keeping biosensor microorganisms alive and active.,"

Current opinion in biotechnology 17(1), 43–9 (2006).

[14]   Vrikkis, R.M., Fraser, K.J., Fujita, K., Macfarlane, D.R., and Elliott, G.D., "Biocompatible ionic liquids: a new approach for stabilizing proteins in liquid formulation.," Journal of biomechanical engineering 131(7), 074514 (2009).

[15]   Weaver, K.D., Vrikkis, R.M., Van Vorst, M.P., Trullinger, J., Vijayaraghavan, R., Foureau, D.M., McKillop, I.H., MacFarlane, D.R., Krueger, J.K., et al., "Structure and function of proteins in hydrated choline dihydrogen phosphate ionic liquid.," Physical chemistry chemical physics : PCCP 14(2), 790–801 (2012).

[16]   Fujita, K., MacFarlane, D.R., and Forsyth, M., "Protein solubilising and stabilising ionic liquids.," Chemical communications (Cambridge, England) 70(38), 4804–4806 (2005).

[17]   Schröder, C., "Proteins in Ionic Liquids: Current Status of Experiments and Simulations.," Topics in current chemistry (Cham) 375(2), 25 (2017).

[18]   Cellemme, S.L., Van Vorst, M., Paramore, E., and Elliott, G.D., "Advancing microwave technology for dehydration processing of biologics.," Biopreservation and biobanking 11(5), 278–84 (2013).

[19]   Beisser, D., Grohme, M.A., Kopka, J., Frohme, M., Schill, R.O., Hengherr, S., Dandekar, T., Klau, G.W., Dittrich, M., et al., "Integrated pathway modules using time-course metabolic profiles and EST data from Milnesium tardigradum.," BMC systems biology 6(1), 72 (2012).

[20]   Crowe, J.H., Carpenter, J.F., and Crowe, L.M., "The role of vitrification in anhydrobiosis.," Annual review of physiology 60, 73–103 (1998).

[21]   Elliott, G.D., Chakraborty, N., and Biswas, D., "Anhydrous preservation of Mammalian cells: cumulative osmotic stress analysis.," Biopreservation and biobanking 6(4), 253–60 (2008).

[22]   Crowe, J., "Stabilization of Dry Mammalian Cells: Lessons from Nature 1," Integrative and Comparative Biology 45(5), 810–820 (2005).

[23]   Yu, L., "Amorphous pharmaceutical solids: preparation, characterization and stabilization," Advanced Drug Delivery Reviews 48(1), 27–42 (2001).

[24]   Einfal, T., Planinšek, O., and Hrovat, K., "Methods of amorphization and investigation of the amorphous state.," Acta pharmaceutica (Zagreb, Croatia) 63(3), 305–34 (2013).

[25]   Crowe, J.H., and Crowe, L.M., "Preservation of mammalian cells-learning nature's tricks.," Nature biotechnology 18(2), 145–6 (2000).

[26]   Allison, S.D., Chang, B., Randolph, T.W., and Carpenter, J.F., "Hydrogen

Bonding between Sugar and Protein Is Responsible for Inhibition of Dehydration-Induced Protein Unfolding," Archives of Biochemistry and Biophysics 365(2), 289–298 (1999).

[27] Champion, D., Le Meste, M., and Simatos, D., "Towards an improved understanding of glass transition and relaxations in foods: molecular mobility in the glass transition range," Trends in Food Science & Technology 11(2), 41–55 (2000).

[28] Chen, B., Fowler, A., and Bhowmick, S., "Forced and natural convective drying of trehalose/water thin films: implication in the desiccation preservation of Mammalian cells.," Journal of biomechanical engineering 128(3), 335–46 (2006).

[29] Brostow, W., Chiu, R., Kalogeras, I.M., and Vassilikou-Dova, A., "Prediction of glass transition temperatures: Binary blends and copolymers," Materials Letters 62(17–18), 3152–3155 (2008).

[30] Roberts, T. V, Lawless, M., Bali, S.J., Hodge, C., and Sutton, G., "Surgical outcomes and safety of femtosecond laser cataract surgery: a prospective study of 1500 consecutive cases.," Ophthalmology 120(2), 227–33 (2013).

[31] Kent, K.M., and Graber, E.M., "Laser tattoo removal: a review.," Dermatologic surgery : official publication for American Society for Dermatologic Surgery [et al.] 38(1), 1–13 (2012).

[32] Anderson, R., and Parrish, J., "Selective photothermolysis: precise microsurgery by selective absorption of pulsed radiation," Science 220(4596), 524–527 (1983).

[33] Roggan, A., Friebel, M., Do Rschel, K., Hahn, A., and Mu Ller, G., "Optical Properties of Circulating Human Blood in the Wavelength Range 400-2500 nm.," Journal of biomedical optics 4(1), 36–46 (1999).

[34] Tan, O.T., Sherwood, K., and Gilchrest, B.A., "Treatment of children with port-wine stains using the flashlamp-pulsed tunable dye laser.," The New England journal of medicine 320(7), 416–21 (1989).

[35] Poetke, M., and Berlien, H.-P., "Laser treatment in hemangiomas and vascular malformations," Medical Laser Application 20(2), 95–102 (2005).

[36] Hale, G.M., and Querry, M.R., "Optical constants of water in the 200-nm to 200-μm wavelength region," Appl. Opt. 12(3), 555–563 (1973).

[37] Vogel, A., and Venugopalan, V., "Mechanisms of Pulsed Laser Ablation of Biological Tissues," Chemical Reviews 103(2), 577–644 (2003).

[38] Gelderblom, H., "Fluid flow in drying drops," Universiteit Twente (2013).

[39] Hu, H., and Larson, R.G., "Analysis of the Effects of Marangoni Stresses on the

Microflow in an Evaporating Sessile Droplet," Langmuir 21(9), 3972–3980 (2005).

[40]   Deegan, R., Bakajin, O., Dupont, T., Huber, G., Nagel, S., and Witten, T., "Contact line deposits in an evaporating drop," Physical Review E 62(1), 756–765 (2000).

[41]   Olszak, A., "Lateral scanning white-light interferometer."

[42]   Schmit, J., Metrology, V., Creath, K., and Wyant, O.J.C., "Surface Profilers, Multiple Wavelength, and White Light Intereferometry."

[43]   Chakraborty, N., "Towards dry preservation of mammalian cells at ambient temperature: Modulating solution effects injury - ProQuest," University of North Carolina at Charlotte (2008).

[44]   Saleki-Gerhardt, A., "Non-Isothermal and Isothermal Crystallization of Sucrose from the Amorphous State," Pharmaceutical Research : An Official Journal of the American Association of Pharmaceutical Scientists 11(8), 1166–1173 (1994).

[45]   Mazzobre, M.F., Aguilera, J.M., and Buera, M.P., "Microscopy and calorimetry as complementary techniques to analyze sugar crystallization from amorphous systems," Carbohydrate Research 338(6), 541–548 (2003).

[46]   "Raman Spectroscopy," University of Michigan, Ann Arbor, pp. 1–6 (2006).

[47]   Rostron, P., and Gerber, D., "Raman Spectroscopy, a review," INternational Journal of Engineering and Technical Research 6(1), 50–64 (2016).

[48]   Hartel, R.W., and Shastry, A. V., "Sugar crystallization in food products," Critical Reviews in Food Science and Nutrition 30(1), 49–112 (1991).

[49]   Sobac, B., and Brutin, D., "Desiccation of a sessile drop of blood: Cracks, folds formation and delamination," Colloids and Surfaces A: Physicochemical and Engineering Aspects 448, 34–44 (2014).

[50]   Caddock, B.D., and Hull, D., "Influence of humidity on the cracking patterns formed during the drying of sol-gel drops" 3(2), 825–834.

[51]   Ragoonanan, V., and Aksan, A., "Heterogeneity in Desiccated Solutions: Implications for Biostabilization," Biophysical Journal 94(6), 2212–2227 (2008).

[52]   Evans, A.A., Cheung, E., Nyberg, K.D., and Rowat, A.C., "Wrinkling of milk skin is mediated by evaporation," Soft Matter (2017).

[53]   Tuschel, D., "Why Are the Raman Spectra of Crystalline and Amorphous Solids Different?," Spectroscopy 32(3), 26–33 (2017).

[54] Romanov, V., Davidoff, S.N., Miles, A.R., Grainger, D.W., Gale, B.K., and Brooks, B.D., "A critical comparison of protein microarray fabrication technologies.," The Analyst 139(6), 1303–26 (2014).

[55] Adams, G., "Lyophilization of vaccines: current trends.," Methods in molecular medicine 87, (2003).

[56] Chang, L.L., Shepherd, D., Sun, J., Ouellette, D., Grant, K.L., Tang, X.C., and Pikal, M.J., "Mechanism of protein stabilization by sugars during freeze-drying and storage: native structure preservation, specific interaction, and/or immobilization in a glassy matrix?," Journal of pharmaceutical sciences 94(7), 1427–44 (2005).

[57] Young, M.A., Antczak, A.T., Elliott, G.D., and Trammell, S.R., "Light assisted drying (LAD) for protein stabilization: optimization of laser processing parameters," in Proc. SPIE 10081, Front. Biol. Detect. From Nanosensors to Syst. IX, A. Danielli, B. L. Miller, and S. M. Weiss, Eds., 100810R (2017).

[58] Young, M.A., McKinnon, M.E., Elliott, G.D., and Trammell, S.R., "Light assisted drying (LAD) for protein stabilization: optical characterization of samples," in Proc. SPIE 10485, Opt. Biophotonics Low-Resource Settings IV, D. Levitz, A. Ozcan, and D. Erickson, Eds., 104850W (2018).

[59] Potschka, M., "Universal calibration of gel permeation chromatography and determination of molecular shape in solution," Analytical Biochemistry 2(1), 47–64 (1987).

[60] Parmar, A.S., and Muschol, M., "Hydration and hydrodynamic interactions of lysozyme: effects of chaotropic versus kosmotropic ions.," Biophysical journal 97(2), 590–8 (2009).

[61] Lopez-Corcuera, B., Alc&ntara, R., Vhzquez, J., and Aragons, C., "Hydrodynamic Properties and Immunological Identification of the Sodium-and Chloride-coupled Glycine Transporter*," THE Jouarra~ OF BIOLOCWAL CHEMISTRY 268(3), 2239–2243 (1993).

[62] Worthington, K., and Worthington, V., "Worthington Enzyme Manual," Worthington Biochemical Corporation (2011).

[63] Blumlein, A., and McManus, J.J., "Reversible and non-reversible thermal denaturation of lysozyme with varying pH at low ionic strength," Biochimica et Biophysica Acta (BBA) - Proteins and Proteomics 1834(10), 2064–2070 (2013).

APPENDIX: PUBLICATIONS

Young, M.A., Elliott, G.D., and Trammell, S.R., "Light-assisted drying for protein stabilization," J. Biomed. Opt. (submitted)

Young, M.A., McKinnon, M.E., Elliott, G.D., and Trammell, S.R., "Light assisted drying (LAD) for protein stabilization: optical characterization of samples," in Proc. SPIE 10485, Opt. Biophotonics Low-Resource Settings IV, 104850W (2018).

Young, M.A., Antczak, A.T., Elliott, G.D., and Trammell, S.R., "Light assisted drying (LAD) for protein stabilization: optimization of laser processing parameters," in Proc. SPIE 10081, Front. Biol. Detect. From Nanosensors to Syst. IX, 100810R (2017).

Young, M.A., Van Vorst, M., Elliott, G.D., and Trammell, S.R., "Light-assisted drying (LAD) of small volume biologics: a comparison of two IR light sources," in Proc. SPIE 9706, Opt. Interact. with Tissue Cells XXVII, 97060F (2016).

Case, J.R., Young, M.A., Dréau, D., and Trammell, S.R., "Noninvasive enhanced mid-IR imaging of breast cancer development in vivo," Journal of Biomedical Optics 20(11), 116003 (2015).

Case, J., Young, M., Keanini, R., and Trammell, S., "Using LED sources to selectively heat blood for enhanced mid-IR imaging of vascular structures," in Biomed. Opt. 2014, BS5A.1 (2014).

Case, J.R., Trammell, S.R., Young, M.A., Israel, U., and Crown, M.X., "Heat as a contrast agent to enhance thermal imaging of blood vessels," in Proc. SPIE 8565, Photonic Ther. Diagnostics IX, 85654H (2013).